11640 *Biochemistry* **2009,** *48,* 11640–11654
DOI: 10.1021/bi901573b

BIOCHEMISTRY
including biophysical chemistry & molecular biology
Article

Metal Binding Affinities of *Arabidopsis* Zinc and Copper Transporters: Selectivities Match the Relative, but Not the Absolute, Affinities of their Amino-Terminal Domains[†,‡]

Matthias Zimmermann,[§,∥] Oliver Clarke,[⊥,#] Jacqui M. Gulbis,[*,#] David W. Keizer,[∥] Renee S. Jarvis,[@] Christopher S. Cobbett,[@] Mark G. Hinds,[*,#] Zhiguang Xiao,[*,§,∥] and Anthony G. Wedd[§,∥]

[§]*School of Chemistry,* [∥]*Bio21 Molecular Science and Biotechnology Institute,* [⊥]*Department of Medical Biology,* [@]*Department of Genetics, University of Melbourne, Parkville, Victoria 3010, Australia, and* [#]*The Walter and Eliza Hall Institute of Medical Research, Parkville, Victoria 3052, Australia*

Received September 8, 2009; Revised Manuscript Received October 31, 2009

ABSTRACT: HMA2, HMA4, and HMA7 are three of the eight heavy metal transporting P_{1B}-type ATPases in the simple plant *Arabidopsis thaliana*. The first two transport Zn^{2+}, and the third transports Cu^{+}. Each protein contains soluble N-terminal metal-binding domains (MBDs) that are essential for metal transport. While the MBD of HMA7 features a CxxC sequence motif characteristic of Cu^{I} binding sites, those of HMA2 and HMA4 contain a CCxxE motif, unique for plant Zn^{2+}-ATPases. The three MBDs HMA2n (residues 1−79), HMA4n (residues 1−96), and HMA7n (residues 56−127) and an HMA7/4n chimera were expressed in *Escherichia coli*. The chimera features the ICCTSE motif from HMA4n inserted in place of the native MTCAAC motif of HMA7n. Binding affinities for Zn^{II} and Cu^{I} of each MBD were determined by ligand competition with a number of chromophoric probes. The challenges of using these probes reliably were evaluated, and the relative affinities of the MBDs were verified by independent cross-checks. The affinities of HMA2n and HMA4n for Zn^{II} are higher than that of HMA7n by a factor of 20−30, but the relative affinities for Cu^{I} are inverted by a factor of 30−50. These relativities are consistent with their respective roles in metal selection and transportation. Chimera HMA7/4n binds Cu^{I} with an affinity between those of HMA4n and HMA7n but binds Zn^{II} more weakly than either parent protein does. The four MBDs bind Cu^{I} more strongly than Zn^{II} by factors of $>10^{6}$. It is apparent that the individual MBDs are not able to overcome the large thermodynamic preference for Cu^{+} over Zn^{2+}. This information highlights the potential toxicity of Cu^{+} in vivo and why copper sensor proteins are ∼6 orders of magnitude more sensitive than zinc sensor proteins. Metal speciation must be controlled by multiple factors, including thermodynamics (affinity), kinetics (including protein−protein interactions), and compartmentalization. The structure of Zn^{II}-bound HMA4n defined by NMR confirmed the predicted ferredoxin $\beta\alpha\beta\beta\alpha\beta$ fold. A single Zn atom was modeled onto a metal-binding site with protein ligands comprising the two thiolates and the carboxylate of the CCxxE motif. The observed ^{113}Cd chemical shift in [^{113}Cd]HMA4n was consistent with a $Cd^{II}S_2OX$ (X = O or N) coordination sphere. The Zn^{II} form of the Cu^{I} transporter HMA7n is a monomer in solution but crystallized as a polymeric chain [$(Zn^{II}$−HMA7n$)_m$]. Each Zn^{II} ion occupied a distorted tetrahedral site formed from two Cys ligands of the CxxC motif of one HMA7n molecule and the amino N and carbonyl O atoms of the N-terminal methionine of another.

P_{1B}-type ATPase transporter proteins pump metal ions across biological membranes. ATP7A and ATP7B, the two known human examples of this class, are Cu^{+} transporters, and mutations are responsible for Menkes and Wilson diseases, respectively (*1*). In contrast, the model plant *Arabidopsis thaliana* contains eight P_{1B}-type ATPases [heavy metal ATPases HMA1−HMA8[1] (Figure 1)] (*2*). Sequence comparisons indicate that HMA1−HMA4 belong to subgroup P_{1B2} and are related to prokaryotic transporters of divalent cations (Zn^{2+}, Cd^{2+}, and Pb^{2+}) and that HMA5−HMA8 belong to subclass P_{1B1} which transports monovalent ions (Cu^{+} and Ag^{+}) (*3*).

HMA2 and HMA4 are closely related in sequence, apparently because of gene duplication during evolution of *A. thaliana* (*4*), and are expressed in the pericycle cells of roots (*5*, *6*). Double mutants *hma2 hma4* accumulate zinc in pericycle cells in roots (*5*) and exhibit zinc deficiency in shoots (*6*), consistent with essential roles in root-to-shoot translocation of zinc. In addition, in the zinc hyper-accumulator species *Arabidopsis halleri*, HMA4 is required for accumulation of zinc in the shoots and for overall hypertolerance to zinc and cadmium (*7*). The N-terminal domains of HMA2 and HMA4 are essential for zinc transport (*8*, *9*). In contrast, loss of the C-terminal domain of HMA2 had little

[†]A.G.W. thanks the Australian Research Council for support under Grant A29930204. M.Z. thanks the University of Melbourne and Ormond College for postgraduate scholarships.

[‡]Coordinates deposited in the Protein Data Bank as entries 2KKH and 3DXS.

*To whom correspondence should be addressed. Z.X.: e-mail, z.xiao@unimelb.edu.au; fax, +61 3 9347 5180; phone, +61 3 8344 2377. J.M.G.: e-mail, jgulbis@wehi.edu.au; fax, +61 3 9347 0852; phone, +61 3 9345 2555. M.G.H.: e-mail, mhinds@wehi.edu.au; fax, +61 3 9347 0852; phone, +61 3 9345 2555.

[1]Abbreviations: Bca, bicinchoninic anion; Bcs, bathocupröine disulfonate; Dtnb, 5,5-dithiobis(2-nitrobenzoic acid); DTT, dithiothreitol; Edta, *N*,*N*,*N*′,*N*′-ethylenediaminetetraacetic acid; Egta, ethylene glycol *O*,*O*′-bis(2-aminoethyl)-*N*,*N*,*N*′,*N*′-tetraacetic acid; ESI-MS, electrospray ionization mass spectrometry; GuHCl, guanidinium chloride; HMA, heavy metal ATPase; Hepes, *N*-(2-hydroxyethyl)piperazine-*N*′-2-ethanesulfonic acid; IPTG, isopropyl β-thiogalactopyranoside; MBD, metal-binding domain; MBM, metal-binding motif; Mes, 2-(*N*-morpholino)ethanesulfonic acid; Mf2, mag-fura-2; Par, 4-(2-pyridylazo)resorcinol; Mops, 3-(*N*-morpholino)propanesulfonic acid; Tcep, tris(2-carboxyethyl)phosphine; Tpen, *N*,*N*,*N*′,*N*′-tetrakis(2-pyridylmethyl)ethylenediamine; Tris, tris(hydroxymethyl)aminoethane.

 Published on Web 11/02/2009

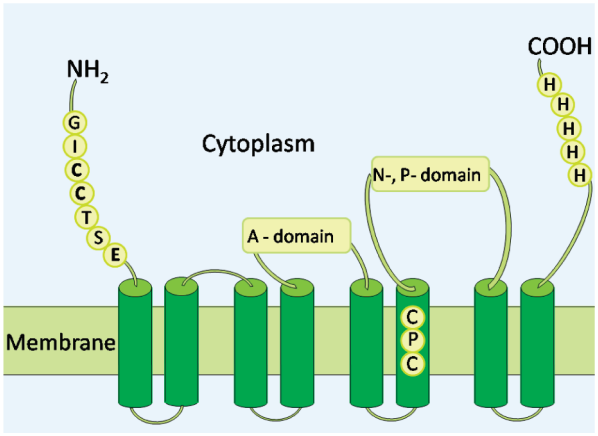

FIGURE 1: Cartoon of the membrane topology of a P_{1B}-type ATPase such as HMA4. Highlighted are the CCxxE sequence in the N-terminus and the histidine-rich C-terminus, both of which are involved in metal binding. The CPC sequence in transmembrane segment 6 is essential for translocation of the metal ion through the membrane.

effect on zinc translocation in planta (*9*), although certain deletions in this domain had an effect when HMA4 was expressed in yeast (*8*, *10*).

HMA5−HMA8 are involved in copper transport (*3*, *11*). Mutants lacking HMA7 (also known as RAN1) are defective in ethylene signaling, and HMA7 is proposed to deliver copper to ethylene receptors after receiving it from the metal chaperone AtCCH1 (*12*). HMA5−HMA8 each feature one or two CxxC sequences in their N-terminal domains (*3*). This metal-binding motif (MBM) within a $\beta\alpha\beta\beta\alpha\beta$ ferredoxin fold is common in Cu^{+} binding proteins such as the metallochaperone Atox1 and the N-terminal domains of ATP7A and ATP7B. In contrast, the N-terminal domains of HMA2−HMA4 (HMA2n−HMA4n, respectively) contain the MBM CCxxE motif which may be specific for Zn^{2+} (*6*, *13*, *14*). An isolated HMA2n domain was reported to bind Zn^{II} with a K_D of 0.18 μM, but its affinity for Cu^{I} appeared to be weaker (K_D = 13 μM) (*13*). Analysis of variant forms indicated that the conserved Glu residue, in addition to the two adjacent Cys residues, was a ligand for Zn^{II}. One Cys residue only with the Glu residue was proposed to be involved in the binding of Cu^{I} (*13*).

The presence of both Zn and Cu transporting P_{1B}-type ATPases in *A. thaliana* provided an opportunity to compare the metal binding selectivities of their soluble N-terminal MBDs under the same conditions. This work isolated and characterized those of Zn transporters HMA2 (residues 1−79) and HMA4 (residues 1−96) and the first of the two tandem MBDs of Cu transporter HMA7 (residues 56−127). In addition, a protein chimera (HMA7/4n) was generated in which the MBM (MTCAAC) in HMA7n was replaced by the equivalent motif (ICCTSE) in HMA4n. The metal binding affinities were determined by ligand competition with the popular Zn^{II} probes mag-fura-2 (Mf2) and 4-(2-pyridylazo)resorcinol (Par) and the Cu^{I} probes bicinchoninic acid (Bca) and bathocupröine disulfonate (Bcs). Their structures are shown in Figure 2. The challenges of using these probes reliably are discussed. The relative affinities of the MBDs were verified via direct competition for the same MBD by Cu^{+} and Zn^{2+} under a variety of conditions. The molecular structures of Zn^{II}−HMA4n and Zn^{II}−HMA7n were determined by NMR spectroscopy and X-ray crystallography, respectively, and were compared to provide insights into the structural basis for the differences in their metal binding properties. The combined

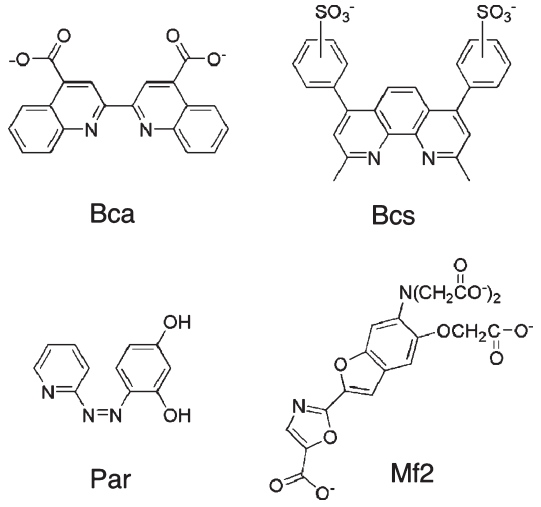

FIGURE 2: Metal probes employed in this study.

data provide valuable information about metal speciation in living cells. A preliminary account of this work has appeared (*15*).

EXPERIMENTAL PROCEDURES

Materials and General Methods. Chemicals and reagents (analytical grade) were purchased from Sigma except for mag-fura-2 (Molecular Probes). Standards for inductively coupled plasma optical emission spectroscopy (ICP-OES) were from CHOICE Analytical Pty Ltd. Unless otherwise stated, characterization and manipulation of all protein samples were conducted anaerobically in deoxygenated buffers in a glovebox ([O_2] < 2 ppm). The samples were transferred in sealed containers for characterization.

Construction of Expression Plasmids. DNA sequences encoding the N-terminal MBDs of HMA2 (HMA2n, residues 1−79), HMA4 (HMA4n, residues 1−96), and HMA7 (HMA7n, residues 56−127) were amplified by PCR from a cDNA library of *A. thaliana*. PCR primers (see Table S1 of the Supporting Information) were designed with an *Nde*I restriction site incorporated in each forward primer and a *Bam*HI site and a stop codon incorporated in each reverse primer to facilitate DNA cloning and protein expression. An extra codon (TGG) was incorporated before the stop codon in the reverse primer for HMA7n to introduce an extra Trp residue at the C-terminus to increase the molar absorptivity ε_{280}. Each PCR product was doubly digested with *Nde*I and *Bam*HI and cloned into expression vector pET11a (Novagen) which was predigested with the same restriction enzymes. A HMA7/4n chimera protein was also designed in which the MBM of HMA7n (MTCAAC) was replaced with the equivalent motif (ICCTSE) present in HMA2 and HMA4. The chimeric gene was assembled from two overlapping PCR products on the HMA7n template with primers incorporating the sequence encoding the ICCTSE sequence (Table S1 of the Supporting Information). DNA sequencing analysis confirmed that each gene sequence was inserted correctly into the expression vector. The four expression plasmids are designated as pET11a-HMA2n, -HMA4n, -HMA7n, and -HMA7/4n.

Protein Expression and Purification. The expression plasmids were maintained in *Escherichia coli* DH5α cells and transformed into *E. coli* BL21(DE3) CodonPlus cells (Stratagene) for protein expression. Each liter of 2YT medium containing ampicillin (100 mg) and chloramphenicol (34 mg) was

inoculated with an overnight culture (10 mL) of the relevant transformed CodonPlus cells. After the cells were grown aerobically with vigorous shaking at 37 °C to an OD_{600} of ~1, IPTG was added to a final concentration of 0.5 mM to induce protein expression. The cultures were grown further at ~30 °C for 3−4 h or at room temperature (~22 °C) overnight before being harvested by centrifugation. The harvested cells were disrupted with lysozyme or with a French press in Tris-HCl buffer (20 mM; pH 8; Edta, 1 mM), and extracts were clarified by centrifugation.

We purified proteins HMA2n and HMA4n by loading the extract onto a cation-exchange CM-52 column (2.6 cm × 15 cm) that had been equilibrated with Mops buffer (50 mM, pH 7.0). The bound proteins were eluted with a NaCl gradient from 0 to 0.3 M NaCl in the same buffer. Each protein eluted as a dominant protein peak in the salt concentration range of 0.1−0.15 M. The protein fractions were pooled, concentrated, and purified further on a Superdex-75 FPLC gel-filtration column in 50 mM Tris-HCl buffer (pH 8.0) (100 mM NaCl and 5 mM DTT). A sample of HMA4n enriched with ^{13}C and ^{15}N was produced similarly from cells grown in a minimal M9 medium supplemented with $[^{15}N]NH_4Cl$ and [^{13}C]glucose.

We purified HMA7n and the HMA7/4n chimera by loading the extract onto an anion-exchange DE-52 column (2.6 cm × 15 cm) that was pre-equilibrated in Tris-HCl buffer (50 mM, pH 8.0). The bound proteins were eluted with a NaCl gradient from 0 to 0.5 M in the same buffer. Protein fractions were identified by SDS−PAGE and were concentrated for further purification on the Superdex-75 FPLC column as described above.

Yields per liter of culture were as follows: 25 mg of HMA2n, 60 mg of HMA4n, 130 mg of HMA7n, and 60 mg of HMA7/4n. Purities were estimated by SDS−PAGE to be >95%. ESI-MS confirmed the protein identity with the first Met residue being removed for HMA2n and HMA4n (Table S2 of the Supporting Information). All proteins were isolated in their apo forms with no detectable content of zinc or copper. To generate metalated forms, apoprotein (150 μL, 0.5 mM) was incubated for 1 h under anaerobic conditions with 3 equiv of Zn^{2+} or $[Cu^{I}(MeCN)_4]^+$. Excess reagents were removed with a Bio-Del P-6 DG gel desalting column (Bio-Rad).

The aggregation states of both apo and Zn^{II} forms of HMA4n and HMA7n were selected for analysis via elution on an analytical Superdex-75 gel-filtration column (HR10/30, Pharmacia) at a flow rate of 0.7 mL/min in 20 mM Mops buffer (pH 7.3) with 100 mM NaCl. The column was calibrated with Blue Dextran (2000 kDa), albumin (67 kDa), ovalbumin (43 kDa), chymotrypsinogen A (25 kDa), and ribonuclease A (13.7 kDa) as standards (Amersham Pharmacia).

Physical Measurements. UV−visible spectra were recorded on a Varian Cary 300 spectrophotometer in dual-beam mode with quartz cuvettes with a path length of 0.5 or 1 cm. ESI mass spectra were recorded on an Agilent Quadrupole-Time of Flight mass spectrometer in the positive ion mode with a fragmentor voltage of 250 V and a skimmer voltage of 65 V at a flow rate of 0.25 μL/min. The diluted samples were mixed with an equal volume of MeOH containing 0.1% formic acid just before delivery to the electrospray probe. The average molar masses were obtained by application of a deconvolution algorithm to the recorded spectra and were calibrated with horse heart myoglobin (16951.5 Da).

Concentration Assays. The concentration of each apoprotein solution was estimated from absorption values at 280 nm. The molar absorptivities (ε_{280}) derived from protein primary sequences were 1400, 8500, and 5500 M^{-1} cm^{-1} for HMA2n, HMA4n, and HMA7n (or HMA7/4n), respectively. These values were confirmed by a thiol assay of the fully reduced apoproteins with Ellman's reagent, 5,5-dithiobis(2-nitrobenzoic acid) (Dtnb). Each apoprotein molecule in its fully reduced form contained two free cysteine thiols that reacted quantitatively with Dtnb, releasing the chromophore 5-mercapto-2-nitrobenzoate (λ_{max} = 418 nm; ε = 13600 M^{-1} cm^{-1}). Fully reduced apoprotein samples were prepared by overnight incubation with excess reductant DTT, followed by a buffer change into 20 mM Mops buffer (pH 7.3) with 100 mM NaCl via a desalting column under anaerobic conditions. All protein samples used for the metal affinity study were confirmed to be fully reduced by analysis of free thiol content.

Stock solutions of $[Cu^{I}(MeCN)_4]^+$, $Cu^{2+}{}_{aq}$, and ligands Edta, Egta, Bca, and Bcs were standardized according to protocols described previously (*51*). A $Zn(NO_3)_2$ standard (15.3 mM) was purchased from Aldrich. Working solutions of the ligand Par were prepared freshly by dilution of a stock solution (~5 mM, pH 10, stored in aliquots at −20 °C) with buffer and calibrated by titration with the Zn^{2+} standard. Par reacts quantitatively with Zn^{2+} to form a 1:2 complex with intense absorption around 500 nm (*18*, *55*). Concentrations of Mf2 solutions were estimated via absorbance at 366 nm using the reported molar absorptivity ε of 2.99 × 10^4 M^{-1} cm^{-1} (*16*). The latter value was confirmed by titration with the Zn^{2+} standard.

Concentrations of metalated proteins were estimated via a thiol assay with Dtnb in the presence of the metal chelator Edta (50 equiv). Control assays with apoprotein samples with and without added Zn^{2+} and Cu^{+} confirmed complete removal of metal ions from the proteins by Edta and release of free cysteine thiols via incubation of the assay mixture for 10 min. Released Cu^{+} is trapped oxidatively as Cu^{II}(Edta) by Edta and residual dioxygen in the reaction solutions. The Zn^{2+} concentration in each isolated Zn^{II}−protein sample was determined spectroscopically with reagent Par. Bound Zn^{II} was released by denaturing the protein with a guanidinium hydrochloride solution (GuHCl) and blocking the Cys residues with iodoacetamide. Briefly, Par reagent (50 equiv), iodoacetamide (10 equiv), and GuHCl (final concentration of 4 M) were added to the sample in Mops buffer (50 mM, pH 7.3). After incubation for 2 h, the Zn^{2+} concentration was estimated by the absorbance value at 500 nm relative to that of a standard Zn^{2+} solution under the same conditions. The Cu^{I} concentrations in the isolated Cu^{I}−protein samples were determined similarly except that the Par reagent was replaced with Bcs reagent (1 mM) that reacts with Cu^{+} specifically and quantitatively under the conditions to produce the anionic complex $[Cu^{I}(Bcs)_2]^{3-}$ (*56*). These spectroscopic approaches to Zn^{2+} and Cu^{+} quantification were verified by independent analysis of selected protein samples with ICP-OES.

Estimation of Zn^{II} and Cd^{II} Binding Affinities. Two independent approaches were used for Zn^{II}. The first involved direct competition for Zn^{II} between the apoprotein and the chromophoric ligand Mf2 according to eq 1 (see Results). Free Mf2 ligand exhibits an intensive absorbance at 366 nm (ε = 2.99 × 10^4 M^{-1} cm^{-1}) which, upon reaction with excess Zn^{2+}, blue-shifts to 325 nm with little residual absorbance remaining at 366 nm (ε = 1.88 × 10^3 M^{-1} cm^{-1}). The protein components of both apo and Zn^{II} forms have no absorbance at 366 nm. Consequently, the free Mf2 concentration in eq 1 can be estimated from the absorbance at 366 nm. Mass balancing allowed estimation of other equilibrium concentrations in eq 1

and thus $K_D(Zn^{II}P)$ from eq 2 using the known value of K_D for $[Zn\text{-}Mf2]^{2-}$ (2.0×10^{-8} M at pH 7.0−7.8) (*16*). The experiments were performed by monitoring changes in solution spectra upon titration of the Zn^{2+} standard into solutions of Mf2 alone or into a mixture of Mf2 and varying concentrations of apoprotein in 50 mM Mops buffer (pH 7.3) with 100 mM NaCl.

The second approach involved competition for Zn^{II} between apoprotein and divalent metal ligand Par according to eq 3. Zn^{2+} reacts with excess Par to produce the 1:2 "$Zn(Par)_2$" complex that absorbs intensively around 500 nm ($\varepsilon \sim 80000\ M^{-1}\ cm^{-1}$ at pH 7.3), while the Par ligand itself absorbs only weakly at this position ($\varepsilon \sim 1400\ M^{-1}\ cm^{-1}$). Thus, the $Zn(Par)_2$ concentration in eq 3 may be obtained from the absorbance at 500 nm with background reference to the free Par ligand solution at the same concentration and, accordingly, $K_D(Zn-P)$ from eq 4. However, the high pH sensitivity of both the formation constant (β_2) and the molar absorptivity (ε) of $Zn(Par)_2$ prevents a reliable estimation of $K_D(Zn-P)$ from eqs 3 and 4 by direct competition with Par alone. Calibration of the binding affinity of Par with a spectroscopically silent ligand such as Egta with a known affinity under the same conditions via eqs 5 and 6 allows cancellation of the uncertainties associated with β_2 and ε and estimation of $K_D(Zn-P)$ via eq 7.

Experiments were performed under anaerobic conditions in 50 mM Tris-HCl buffer (pH 8.4) with 100 mM NaCl or in 50 mM Na-Mops buffer (pH 7.3) with 100 mM NaCl. Solutions containing $Zn(Par)_2$ were prepared by mixing Par and Zn^{2+} in the [Par]:[Zn] molar ratio range of 5−10, followed by addition of known quantities of apoprotein or Egta (5−50 μM) to set up the competition. Equilibrium was attained after incubation for ~10 min, and the equilibrium concentration of $Zn(Par)_2$ was estimated spectrophotometrically relative to a control solution without the competitors.

The affinity of HMA4n for Cd^{II} was estimated by direct metal competition for protein between Cd^{2+} and Zn^{2+} ions. Addition of equimolar excesses (2 equiv) of two metal ions to an apo-HMA4n solution followed by removal of unbound metal ions on a desalting column provided metalated protein Cd_xZn_{1-x}−HMA4n. The metal contents were estimated by ICP-OES after digestion of the protein samples at 85 °C in HNO_3 (10%) for 24 h.

Estimation of Cu^I Binding Affinities. The two Cu^I-specific reagents Bca and Bcs were employed according to the relationships of eqs 9 and 10. Experiments were conducted under anaerobic conditions in 50 mM Mops buffer (pH 7.3) with 100 mM NaCl with protocols following those reported previously (*23*, *24*). Each reaction in eq 9 was performed with at least two different concentrations of ligand L under otherwise identical conditions, and the resultant solution spectra were compared to judge if the reaction was in equilibrium competition.

Direct Competition of Cu^+ and Zn^{2+} for HMA2n and HMA4n. Two types of competition were set up. The first was to allow Cu^+ and Zn^{2+} both in "free" unbound form to compete for HMA2n or HMA4n directly. This is equivalent to the competition between Cd^{2+} and Zn^{2+} given above. The metal content of the isolated proteins was analyzed for Cu^I with Bcs and for Zn^{II} with Par. Control experiments demonstrated that Zn^{2+} did not interfere with analysis of the total copper content, but analysis with Par provided the total content of divalent metal ions (including Cu^{2+} derived from Cu^+ under the oxidizing conditions). The Zn^{2+} content was estimated after subtraction of the calculated contribution to the total absorbance from $[Cu^{II}(Par)_2]$, and this was confirmed using ICP-OES.

The second approach was to allow free Zn^{2+} to compete with the Cu^I bound in $[Cu^I(Bca)_2]^{3-}$ for HMA4n via eq A:

$$Cu^I\text{−HMA4n} + Zn^{2+} + 2Bca^{2-} \rightleftharpoons [Cu^I(Bca)_2]^{3-} + Zn^{II}\text{−HMA4n} \quad \text{(A)}$$

The experiments were conducted in both directions. In the forward reaction, apo-HMA4n (10 μM) was first overloaded with 2 equiv of Cu^+ (20 μM) in the presence of Bca (45 μM) that led to loading of HMA4n with 1 equiv of Cu^I only and the excess Cu^+ being trapped as $[Cu^I(Bca)_2]^{3-}$. A duplicate solution was prepared but with a final addition of extra Zn^{2+} ions (20 μM). Comparison of the absorbance values at 562 nm of these two solutions allowed monitoring of the destination of the added Zn^{2+} ions. In the reverse reaction, a third solution of identical ligand composition was prepared but with apoprotein preloaded with Zn^{2+} in the presence of Bca, followed by addition of Cu^+. A comparison of the visible spectrum of this solution with those of the first two solutions tested the possibility that protein-bound Zn^{II} might prevent quantitative binding of Cu^+ to the protein.

X-ray Crystallography. Crystal Growth and Analysis. Sparse matrix vapor diffusion crystallization trials were conducted for apo and various metal-loading forms of HMA4n and HMA7n. For each protein, 800 precipitant conditions were screened in 96-well sitting drop trays at 18 °C. Each drop contained 100 nL of protein solution (20 mg/mL; apo or Zn^{2+}-, Cu^+-, Cd^{2+}-, or Hg^{2+}-loaded form) in a buffer containing 20 mM Mops (pH 7.3) and 100 mM NaCl and 100 nL of precipitant solution. Conditions yielding crystals were optimized in 24-well sitting/hanging drop trays, where 1 μL of protein solution was mixed with 1 μL of precipitant solution and equilibrated against a 500 μL reservoir. These procedures led to crystallization of both HMA4n and HMA7n in the presence of Cu^+ and Zn^{2+}. However, only crystals of Zn^{2+}-loaded HMA7n diffracted. These crystals grew within 1 week against a reservoir of 1.2 M lithium chloride and 0.1 M Tris-HCl (pH 8.0).

Prior to being cryocooled in liquid nitrogen, crystals used for data collection were cryoprotected by being streaked through Paratone-N. Data to a resolution limit of 1.7 Å were collected from a single crystal belonging to orthorhombic space group $P2_12_12_1$ (cell dimensions a = 27.368 Å, b = 44.525 Å, and c = 49.220 Å) on beamline X10SA at the Swiss Light Source. The asymmetric unit contains one molecule of HMA7n. Intensity data collected at the Zn^{2+} L(I) edge (λ = 1.284 Å) were processed and scaled using HKL2000 (*57*); collection and refinement statistics are reported in Table 3.

Structure Solution and Refinement. References are provided in the Supporting Information. Anomalous scattering from a specifically bound Zn^{II} ion was used to phase an initial electron density map by single-wavelength anomalous diffraction (SAD) methodology. Using SHELXD, a single Zn^{II} site was located and initial phases were obtained. An initial round of density modification was performed using SHELXE. Further density modification was conducted using the SOLVE/RESOLVE suite, employing solvent flattening and histogram matching protocols implemented in RESOLVE to improve the phases. Model building was conducted using the automated building and refinement capabilities of RESOLVE, followed by further manual editing in COOT. Atomic coordinates were refined using maximum likelihood procedures in REFMAC 5, with alternating cycles of individual anisotropic B factor refinement. The final model contained all residues of the HMA7n protein. Side chains of

residues Arg2 and Glu59 were truncated at Cβ and Cγ, respectively, due to positional disorder. Refinement of 856 non-hydrogen atoms, including 116 water molecules, one Zn^{2+}, and one Li^{+} ion, against 7384 terms (371 additional terms were excluded from refinement and retained as a reference set) in the resolution range of 50.0−1.7 Å converged at an R_{free} of 0.160 and an R_w of 0.142. There are no outliers in the Ramachandran plot (96.6% of the residues in the most favored regions), and root-mean-square deviations (rmsd) of bond lengths and angles are 0.0096 Å and 1.24°, respectively. The average isotropic *B* factor is 9.2 $Å^2$.

NMR Spectroscopy and Spectral Assignments. Full referencing is provided in the Supporting Information. NMR experiments were performed on ^{13}C- and ^{15}N-enriched HMA4n samples (~0.5 mM) prepared in the glovebox in KP_i buffer (50 mM, pH 7.3) containing 5% D_2O and 0.02% NaN_3. Tcep and Edta (each at 0.5 mM) were included in the apo form to ensure full reduction and metal-free conditions. The Zn^{II}− and ^{113}Cd−HMA4n samples were prepared by direct titration of Zn^{2+} or $^{113}Cd^{2+}$ (1 equiv) into apo-HMA4n in the sample buffer.

Spectra were recorded at 25 °C on a Bruker DRX 600 spectrometer equipped with triple-resonance probes and pulsed field gradients operating at 600 MHz, or AV-500 and AV-800 spectrometers equipped with cryogenically cooled probes, operating at 500 and 800 MHz, respectively. A series of heteronuclear three-dimensional (3D) NMR experiments were recorded using ^{13}C- and ^{15}N-labeled HMA4n proteins (*26*). Spectra were processed using TOPSPIN (Bruker AG) and analyzed using XEASY.

Distance and Dihedral Angle Restraints. Distance restraints were measured from the 100 ms mixing time 3D ^{15}N-edited NOESY, ^{13}C-edited NOESY, and 2D NOESY spectra. Hydrogen bond constraints were applied within α-helices and the β-sheet at a late stage of the structure calculation. Both ϕ and ψ backbone torsion angles were derived using TALOS. Dihedral angle restraints for ϕ and ψ angles were used as summarized in Table 4.

Structure Calculation and Analysis. Initial structures were calculated using CYANA 2.1 (*27*) and then refined with Xplor-NIH (version 2.22) (*29*) using radius of gyration, hydrogen bonding, and Ramachandran terms. Structural statistics for the final set of 20 structures, selected from the 256 calculated structures on the basis of their stereochemical energies, are presented in Table 3. PROCHECK_NMR and MOLMOL were used for the analysis of structure quality. The final structures had no experimental distance violations greater than 0.2 Å or dihedral angle violations greater than 5°.

RESULTS

Protein Expression, Purification, and Characterization. Three N-terminal MBDs HMA2n(1−79), HMA4n(1−96), and HMA7n(56−127) from the P_{1B}-type ATPases of *A. thaliana* were expressed at high levels in *E. coli* as was the protein chimera HMA7/4n described above. ESI-MS data confirmed removal of the N-terminal Met residue for both HMA2n and HMA4n, but

Table 1: Analytical Data of Metal Binding Stoichiometries[a]

protein	Zn^{II}[b]	Cd^{II}[b]	Cu^{I}[b]	Cu^{I}[c]
HMA2n	0.98		2.02	1.87
HMA4n	0.97	0.99	2.06	1.05
HMA7n	0.96		1.10	0.98
HMA7/4n chimera	0.92		1.94	1.08

[a]Data are the average of analysis of three independent samples with uncertainties of ±0.05. [b]For isolated samples; protein concentrations were estimated by a thiol assay upon removal of the bound metal ions, and metal concentrations were analyzed by the Zn^{2+} and Cd^{2+} probe Par or the Cu^{+} probe Bcs as detailed in Experimental Procedures. [c]Refers to the number of equivalents of Cu^{I} removed by apoproteins from the chromaphoric complex $[Cu^{I}(Bca)_2]^{3-}$ at 1:3−1:6 Cu^{I}:Bca molar ratios.

Table 3: X-ray Collection and Refinement Statistics for Zn^{II}−HMA7n

Data Collection	
space group	$P2_1\,2_1\,2_1$
cell dimensions *a*, *b*, *c* (Å)	27.374, 44.529, 49.223
wavelength (Å)	1.283
resolution (Å)	1.70 (1.76−1.70)[a]
R_{sym} or R_{merge}	0.092 (0.189)[a]
$I/\sigma I$	23.6 (7.4)[a]
completeness (%)	90 (54)[a]
redundancy	6.6 (3.7)[a]
Refinement	
resolution (Å)	1.70
no. of reflections	7384
R_{work}/R_{free} (5%)	0.142, 0.160
no. of atoms (non-hydrogen)	747
⟨*B* factor⟩ ($Å^2$)	9.2
rmsd	
bond lengths (Å)	0.010
bond angles (deg)	1.24

[a]Values in parentheses are for the highest-resolution shell.

Table 2: Dissociation Constants (K_D) for HMA MBDs[a]

			$K_D(Zn^{II})$ (M)				
protein	MBM	pH	Mf2[b]	Par/Egta[b]	$K_D(Cd^{II})$ (M)	$K_D(Cu^{I})$ [c] (M)	ref
HMA2n(1−75)	ICCTSE	7.0	2.9×10^{-8}[d]		4.4×10^{-8}[d]	1.3×10^{-5}	*13*
HMA2n(1−79)	ICCTSE	7.3	$< 10^{-9}$	$2.5(3) \times 10^{-10}$		$1.9(3) \times 10^{-17}$	this work
HMA4n	ICCTSE	7.3	$< 10^{-9}$	$2.1(6) \times 10^{-10}$	3.5×10^{-11}	$2.9(3) \times 10^{-17}$	this work
HMA7n	MTCAAC	7.3	$4.6(2) \times 10^{-9}$	$5.8(4) \times 10^{-9}$		$6.5(15) \times 10^{-19}$	this work
HMA7/4n chimera	ICCTSE	7.3	$2.5(5) \times 10^{-8}$	$2.5(3) \times 10^{-8}$		$5.7(15) \times 10^{-18}$	this work

[a]The original data and calculations are given in Tables S5−S7 of the Supporting Information. [b]Values were calculated on the basis of a $K_D(Zn^{II}$−Mf2) of 2.0×10^{-8} M (*16*) and a $K_D(Zn^{II}$−Egta) of 1.0×10^{-9} M at pH 7.3 (see Table S3 of the Supporting Information). [c]For the first equivalent of Cu^{I} (high affinity). [d]Note that the reported data for $K_D(Zn^{II})$ (1.8×10^{-7} M) and $K_D(Cd^{II})$ (2.7×10^{-7} M) were based on a $K_A(Zn^{II}$−Mf2) of 1.25×10^{-7} M. For better comparison, these values were converted using the $K_D(Zn^{II}$−Mf2) value reported in ref *16* (see footnote [b]).

Table 4: Summary of Restraints and Structural Statistics for the 20 Lowest-Energy Structures of Zn−HMA4n in 50 mM KP_i buffer (pH 7.3) with 0.02% NaN_3 at 25 °C

no. of experimental constraints	
total	1913
intraresidue	811
sequential ($\|i-j\| = 1$)	283
short-range ($1 < \|i-j\| < 5$)	212
long-range ($\|i-j\| \geq 5$)	377
hydrogen bond	30
dihedral angle (ϕ, 57; ψ, 58)	115
rmsd from experimental distance restraints (Å)	0.016 ± 0.001
rmsd from experimental dihedral angle restraints (deg)	0.28 ± 0.09
rmsd from idealized covalent geometry	
bonds (Å)	0.003 ± 0
angles (deg)	0.42 ± 0.01
impropers (deg)	0.28 ± 0.01
measures of structural quality	
E_{LJ} (kcal/mol)	−320.4 ± 9.6
Procheck percentage of residues in a region of the Ramachandran plot [residues with $S(\phi)$ and $S(\psi) \geq 0.9$: total, 70]	
most favorable	83.4 (91.6)
additionally allowed	10.6 (6.2)
generously allowed	4.5 (1.7)
disallowed	1.5 (0.5)
angular order	
residues with $S(\phi) \geq 0.9$	73
residues with $S(\psi) \geq 0.9$	76
overall G factor	0.35 ± 0.02
no. of bad contacts per 100 residues	8.1 ± 2.2
violations	
experimental distance constraints of > 0.2 Å	0
experimental dihedral constraints of > 5°	0
coordinate precision	

Coordinate Precision

mean pairwise rmsd (Å)	C^α, C, N	all heavy atoms
all residues	8.23 ± 2.68	9.14 ± 2.64
regular secondary structure	0.36 ± 0.09	1.05 ± 0.12

not for HMA7n or HMA7/4n (Table S2 of the Supporting Information). HMA2n and HMA4n are slightly basic and were purified readily by cation-exchange chromatography, followed by gel filtration. HMA7n and the HMA7/4n chimera are acidic and were purified on an anion-exchange resin followed by gel filtration. All four apoproteins eluted cleanly on an analytical gel-filtration column in buffer containing DTT (5 mM) at positions expected for monomeric forms (Figure S1 of the Supporting Information). Reaction with Ellman's reagent Dtnb confirmed the presence of two reduced Cys residues in each isolated apoprotein sample and provided independent confirmation of the apoprotein concentrations estimated from the absorbance spectra. Each apoprotein oxidized slowly in air with formation of disulfide bonds (20−30% oxidation in 24 h). Samples used for metal affinity determinations were routinely checked for thiol content to ensure full reduction.

Addition of excess Zn^{2+}, Cd^{2+}, or Cu^+ (3 equiv) into solutions of fully reduced apoproteins followed by removal of unbound metal ions by a desalting column in the anaerobic glovebox led to the isolation of metalated forms. HMA2n, HMA4n, HMA7n, and the HMA7/4n chimera each bound 1 equiv of Zn^{II} (or Cd^{II}) per protein molecule (Table 1). HMA7n also bound 1 equiv of Cu^I, but HMA2n, HMA4n, and HMA7/4n bound 2 equiv of Cu^I (Table 1). However, when the Cu^+ concentration was buffered by the complex $[Cu(Bca)_2]^{3-}$ (1:3−6 Cu^+:Bca molar ratio), all of the MBDs retained 1 equiv of Cu^+ only while HMA2n continued to bind 2 equiv. HMA2n retained 1 equiv of Cu^+ only when the metal ion was buffered at lower concentrations (1:10−30 Cu^+:Bca molar ratio). It is apparent that each MBD has one site of high affinity but that all except HMA7n have a second site of lower affinity.

Titration of slightly more than 1 equiv of Cu^+ or Zn^{2+} into each apoprotein solution blocked detection of free thiol. Samples in which the Cys residues were oxidized or modified by acetamide exhibited no affinity for either Cu^+ or Zn^{2+}. These results indicate that both Cys residues in each MBM are involved in Cu^I and Zn^{II} coordination. Further quantitative analysis follows below.

Binding of the metals retarded oxidation of the Cys thiols dramatically. For example, after aerobic storage of Zn^{II}−HMA4n and Zn^{II}−HMA7n samples at 4 °C for 1 day, both Cys residues remained fully reduced and bound to Zn^{II}: they were detected quantitatively by Ellman's reagent upon in situ removal of Zn^{II} by Edta. Each protein sample eluted cleanly from an analytical gel-filtration column at positions expected for their respective apoprotein with the Zn^{II} content fully retained (see Figure S1 of the Supporting Information). These results indicate tight binding of the Zn^{II} ion.

Binding Affinities for Zn^{II} and Cd^{II}. The MBDs each bind 1 equiv of Zn^{II}. Quantitative estimation of binding affinities was achieved via ligand competition. Mf2 is a sensitive probe for Zn^{II} which induces spectral changes featuring two tight isosbestic points at 342 and 276 nm (Figure 3a). The absorbance change at 366 nm reports the free Mf2 concentration ($\varepsilon = 2.99 \times 10^4$ M^{-1} cm^{-1}). Titration of Zn^{2+} into Mf2 solution led to a linear decrease in the absorbance at 366 nm with a turning point at a Zn^{II}:Mf2 ratio of ~1.0 with weak residual absorbance [$\varepsilon = 1.88 \times 10^3$ M^{-1} cm^{-1} (Figure 3b, trace i)]. The equivalent titration in the presence of an equimolar concentration of HMA7n in 50 mM Mops buffer (pH 7.3) with 100 mM NaCl provided a steady decrease in absorbance until a Zn^{II}:Mf2 ratio of 2.0 was reached (Figure 3b, trace ii), indicating effective competition between HMA7n (P) and Mf2 for the added Zn^{2+} (see Experimental Procedures for details):

$$[Zn^{II}-Mf2]^{2-} + \text{apo-P} \rightleftharpoons Zn^{II}-P + Mf2^{4-} \quad K_{ex1} \qquad (1)$$

$$K_D(Zn-P) = (K_{ex1})^{-1} K_D(Zn-Mf2) \qquad (2)$$

where $K_D(Zn-Mf2)$ is the known dissociation constant of $[Zn-Mf2]^{2-}$ (2.0×10^{-8} M at pH 7.0−7.8) (*16*). Quantitative analysis of the experimental data via eqs 1 and 2 estimated a K_D of $4.6(2) \times 10^{-9}$ M for Zn^{II}−HMA7n; i.e., HMA7n has a slightly stronger affinity for Zn^{2+} than Mf2 does (Table 2 and Table S5 of the Supporting Information). The equivalent titrations for HMA2n or HMA4n (~1 equiv) induced little initial spectral change until the Zn^{II}:Mf2 ratio approached ~1 (Figure 3b, trace iii), i.e., until HMA2 and HMA4n were almost saturated with Zn^{II}. This behavior is similar to that seen with the high-affinity Zn^{II} ligand Edta (Figure 3b, trace iv). On the other hand, titration of apo-HMA4n (1.1 equiv relative to Zn^{II}) into a solution containing Zn^{II} and Mf2 (1:2) led to a quantitative release of

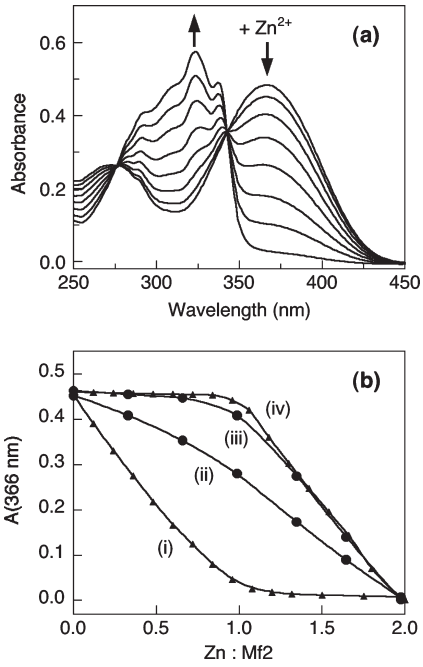

FIGURE 3: Determination of Zn^{II} dissociation constants (K_D) for HMA2n, HMA4n, and HMA7n proteins in 50 mM Mops buffer (pH 7.3) with 100 mM NaCl with the Mf2 probe. The concentration of each reagent was 15.2 μM. (a) Changes in the solution spectrum of a mixture of Mf2 and HMA7n upon titration with Zn^{2+}. (b) Plots of A_{366} (proportional to the free Mf2 concentration) as a function of the Zn^{II}:Mf2 ratio in the presence of (i) Mf2 only, (ii) Mf2 and apo-HMA7n, (iii) Mf2 and apo-HMA4n (or apo-HMA2n), or (iv) Mf2 and Edta.

Mf2 as a free ligand. These experiments demonstrate that the Zn^{II} affinities of both HMA2n and HMA4n are higher than that of HMA7n and are in fact too high to be quantified reliably with the Mf2 probe (Table S3 of the Supporting Information). This probe detects Zn^{II} binding via the absorbance of the free ligand rather than of the metal complex. This imposes an experimental upper limit to the total Mf2 concentration of ~35 μM and narrows its Zn^{2+} buffering range (see Figure S2 of the Supporting Information). Interestingly, equivalent experiments showed that protein chimera HMA7/4n binds Zn^{II} with an affinity lower than that of either of its parent proteins, HMA4n and HMA7n (Table 2).

To estimate the Zn^{II} binding affinities of HMA2n and HMA4n quantitatively, a second chromophoric probe Par was selected (Figure 2). When the Par:Zn^{II} ratio exceeds 2, the ligand reacts quantitatively with Zn^{2+} to form a 1:2 complex, written for the sake of convenience as $Zn(Par)_2$. The complex absorbs ~60 times more intensively around 500 nm than the free ligand does [$\varepsilon \sim 80000$ and 1400 M^{-1} cm^{-1} at pH 7.3, respectively (Figure 4a and Table S5 of the Supporting Information)]. Thus, its advantages as a Zn probe over Mf2 include (i) detection of the $Zn^{II}(Par)_2$ metal complex rather than the free ligand Par, allowing the Par concentration to be varied over the range of 50−1000 μM with minimal impact on detection of metal binding and (ii) the fact that the effective metal buffering range varies with total ligand concentration more widely in the Par system than in the Mf2 system due to formation of a 1:2 complex in the former and a 1:1 complex in the latter (Figure S2 of the Supporting Information). Consequently, Par can buffer Zn^{2+} concentration over a wider range than Mf2, and this allows quantitative comparison of Zn^{II} binding affinities over that wider range. A competition between the two ligands, Par and protein P, is described by

$$Zn(Par)_2 + \text{apo-P} \rightleftharpoons Zn{-}P + 2Par \quad K_{ex3} \tag{3}$$

$$K_{ex3} = \frac{[Zn{-}P][Par]^2}{[Zn(Par)_2][P]} = [K_D(Zn{-}P)]^{-1}(\beta_2)^{-1} \tag{4}$$

where β_2 is the overall formation constant of $Zn(Par)_2$. The equilibrium concentration of $Zn(Par)_2$ in eq 3 may be obtained from the absorbance at 500 nm with reference to a background solution of Par at the same concentration. However, the Par ligand features two ionizable hydroxyl functions, and Zn^{II} binding leads to deprotonation of the less acidic 3′-hydroxyl (pK_a = 12.4) rather than the more acidic 1′-hydroxyl (pK_a = 7.0) (*17*). Using the notation Par = LH_2, the neutral complex $Zn^{II}(HL)_2$ will be in equilibrium with $[Zn^{II}(HL)L]^-$ and $[Zn^{II}(L)_2]^{2-}$. The values of pK_{a1} and pK_{a2} for this system were reported to be 7.7 and 9.3, respectively, in one study (*17*) and 6.45 and 7.55, respectively, in another (*18*). It is apparent that both the formation constant β_2 and the molar absorptivity ε of $[Zn^{II}(Par)_2]$ are pH-dependent in the range of 6−9 and difficult to define accurately and reproducibly. For example, when the pH increases by 2 units from 7 to 9, ε at 500 nm increases by 50% and β_2 by a factor of 10^{10} (see Table S5 of the Supporting Information). Therefore, the relative binding affinities of different proteins for Zn^{II} can be compared quantitatively and reliably only in the same reaction buffer. It is not appropriate to estimate Zn^{2+} affinities by using Par as a competing ligand alone without careful consideration of the influence of pH. This aspect has been ignored in a number of studies (*19*−*22*). The difficulty may be circumvented by calibration of the metal binding affinities of Par and proteins with a spectroscopically silent ligand of known affinity (such as Egta) under the same reaction conditions:

$$Zn(Par)_2 + Egta \rightleftharpoons Zn{-}Egta + 2Par \quad K_{ex5} \tag{5}$$

$$K_{ex5} = \frac{[Zn{-}Egta][Par]^2}{[Zn(Par)_2][Egta]} = [K_D(Zn{-}Egta)]^{-1}(\beta_2)^{-1} \tag{6}$$

$$K_D(Zn{-}P) = K_D(Zn{-}Egta)\frac{K_{ex5}}{K_{ex3}} \tag{7}$$

The uncertainties associated with β_2 and ε with buffer pH are offset because both competitions 3 and 5 are performed in the same reaction buffer which ensures a similar Zn^{II} occupancy on Par. Thus, $K_D(Zn{-}P)$ may be obtained from eq 7 (derived from a combination of eqs 4 and 6) with the known value of K_D-(Zn−Egta) corrected for pH (see Tables S4 and S6 of the Supporting Information).

As demonstrated in panels b and c of Figure 4, changes in the equilibrium positions of eqs 3 and 5 with increasing protein or Egta concentrations may be expressed as a plot of A_{500} versus the molar ratio of total protein (or ligand) to total Zn^{II}. A rapid decrease in A_{500} {proportional to $[Zn(Par)_2]$} with an increasing relative protein concentration indicates strong competition and a high affinity of the protein for Zn^{II}. Variation of the total Par concentration under otherwise identical conditions can alter the equilibrium position of the competition (cf. panels b and c of Figure 4). For example, HMA4n extracts Zn^{II} from Par almost quantitatively at a total Par concentration of 50 μM, but not at 100 μM (Figure 4b, trace i, vs Figure 4c, trace i). On the other

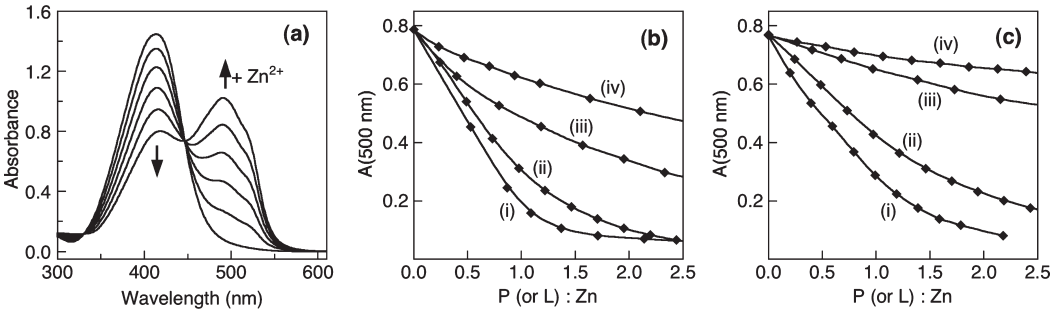

FIGURE 4: Determination of Zn^{II} dissociation constants (K_D) for HMA4n and HMA7n proteins in 50 mM Mops buffer (pH 7.3) with 100 mM NaCl with the probe Par. (a) Changes in the spectrum of a solution containing Par (100 μM) in the presence of increasing Zn^{2+} concentrations of 0, 5, 10, 15, 20, and 25 μM. (b and c) Variation of A_{500} {proportional to $[Zn^{II}(Par)_2]$} with the L:Zn ratio for a $[Par]_{total}$ of 50 (b) or 100 μM (c). $[Zn^{II}]_{total} \sim 10$ μM. For panels b and c: (i) HMA4n (or HMA2n), (ii) Egta, (iii) HMA7n, and (iv) HMA7/4n chimera.

hand, the HMA7/4n chimera competes for Zn^{II} effectively at the lower Par concentration, but not at the higher Par concentration (Figure 4b, trace iv, vs Figure 4c, trace iv). Therefore, effective competition can be ensured by adjustment of the Par:Zn^{II} ratio so that the observed Zn^{II} occupancies on both the proteins and Egta are in the range of 0.2−0.8 while ensuring that A_{500} for $Zn^{II}(Par)_2$ remained >0.1. A series of experiments under such conditions (see Experimental Procedures and Table S6A−C of the Supporting Information for details) provided quantitative estimation of the binding affinities for Zn^{II} of all four protein domains at pH 7.3 on the basis of the known binding affinity of Egta under the same conditions (Table 2). The data demonstrate that the K_D values of the four MBDs increase in the following order (i.e., their affinities for Zn^{II} decrease in that order):

$$\text{HMA2n} \sim \text{HMA4n}\ (10^{-9.7}\ \text{M}) < \text{Egta}\ (10^{-9.0}\ \text{M}) < \text{HMA7n}\ (10^{-8.2}\ \text{M}) < \text{HMA7/4n}\ (10^{-7.6}\ \text{M}) \quad (8)$$

HMA2n and HMA4n bind Zn^{II} more strongly than HMA7n and the HMA7/4n chimera do by factors of ~30 and ~100, respectively. Notably, the K_D values of HMA7n and HMA7/4n estimated via the Par−Egta probe are identical, within the experimental error, to those estimated via the Mf2 probe (Table 2), underscoring the reliability of the approaches adopted in this study.

The affinity of HMA4n for Cd^{II} was estimated by direct metal competition between Zn^{2+} and Cd^{2+} (see Experimental Procedures for details). HMA4n binds Cd^{2+} more strongly than Zn^{2+} by a factor of 6 (Table 2).

Binding Affinities for Cu^I. The two Cu^I-specific probes Bca and Bcs were employed. They each react with Cu^+ to produce air-stable 1:2 anionic complexes, $[Cu^IL_2]^{3-}$ (L = Bca^{2-} or Bcs^{2-}) with intense absorbance maxima in their visible solution spectra but with overall formation constants (β_2) differing by a factor of $10^{2.6}$ (for $[Cu^I(Bca)_2]^{3-}$, $\lambda_{max} = 562$ nm, $\varepsilon = 7900\ M^{-1}\ cm^{-1}$, and $\beta_2 = 10^{17.2}$, and for $[Cu^I(Bcs)_2]^{3-}$, $\lambda_{max} = 483$ nm, $\varepsilon = 13000\ M^{-1}\ cm^{-1}$, and $\beta_2 = 10^{19.8}$) (*23*, *24*). They may compete with a protein for Cu^+ according to eq 9:

$$[Cu^IL_2]^{3-} + \text{apo-P} \rightleftharpoons Cu^I\text{-P} + 2L^{2-} \quad K_{ex9} \quad (9)$$

$$K_D(Cu^IP) = (\beta_2)^{-1}(K_{ex9})^{-1} = (\beta_2)^{-1}\frac{[Cu^IL_2][P]}{[Cu^IP][L]^2} \quad (10)$$

Provided that metal-exchange reaction 9 is an effective competition and that ligand L is in excess, the observed concentration of $[Cu^IL_2]^{3-}$ in solution will depend on the total concentrations of L and protein P, allowing the dissociation constant $K_D(Cu^IP)$ to be estimated via eq 10. On the other hand, if reaction 9 is not in equilibrium and, in addition, protein P binds Cu^+ much more strongly than ligand L does, the $[Cu^IL_2]^{3-}$ concentration will depend on the concentration of P but not on that of L. This allows quantification of the stoichiometry of high-affinity Cu^I binding.

As discussed above (Table 1), experiments with the weaker Cu^I probe Bca demonstrated that the copper-transporting domain HMA7n binds 1 equiv of Cu^I with high affinity (i.e., forward reaction only for eq 9) but that the zinc-transporting domains, HMA2n and HMA4n (including the HMA7/4n chimera), each bind 2 equiv of Cu^I sequentially with different affinities (Table 1). This was confirmed by quantitative analysis with the Bca probe. Titration of Cu^+ into a solution containing HMA4n (10 μM) and Bca (45 μM) did not induce the spectral features characteristic of $[Cu^I(Bca)_2]^{3-}$ at 562 nm until >1 equiv of Cu^+ was added (Figure 5, trace i). This demonstrates that the first equivalent of Cu^I binds to HMA4n with sufficient affinity to prevent its removal by Bca at 45 μM. On the other hand, although a Cu^I_2−HMA4n species was isolated via a desalting column under anaerobic conditions, the Cu^I−HMA4n species cannot compete with the excess Bca for the second equivalent of Cu^+ (Figure 5, trace ii). The use of eq 10 with the experimental data in Figure 5 and the known value of β_2 for $[Cu^I(Bca)_2]^{3-}$ estimated a K_{D1} of $<10^{-15}$ M and a K_{D2} of $>10^{-13}$ M for HMA4n. However, the affinity of HMA2n for the second Cu^+ ion appears to be higher than that of HMA4n, since HMA2n binds almost 2 equiv of Cu^I under conditions when HMA4n (and HMA7/4n) can bind only 1 equiv (Table 1). A modification of the two Cys residues in each protein sample by either alkylation with iodoacetamide or oxidation to a disulfide bond abolishes the affinity for Cu^+ completely, suggesting that both Cu^I ions are bound at a binding site(s) associated with the two Cys residues. This may be a $Cu^I_2(\mu\text{-S-Cys})_2$ binuclear unit similar to that proposed for the metallochaperone Atx1 from *Saccharomyces cerevisiae* (*24*).

The affinities of each MBD for the first equivalent of Cu^I were estimated quantitatively with the second Cu^I-specific probe Bcs which has a higher affinity for Cu^I than the Bca probe does (*23*, *24*). Effective competition for Cu^I was apparent from correlated changes of the Cu^I occupancies on the competitors by variation of the concentration of either Bcs or the protein (Table S7A,B of the Supporting Information). HMA2n and HMA4n compete for Cu^I at the lower Bcs concentration (200 μM) but not at the higher concentration [500 μM (Figure 6b, trace i, vs Figure 6c, trace i)]. In contrast, HMA7n extracts Cu^I from Bcs at the lower Bcs concentration and competes effectively at the

higher Bcs concentration (Figure 6b, trace iii, vs Figure 6c, trace iii). The HMA7/4n chimera binds Cu^I with an affinity between those of its protein parents HMA4n and HMA7n and competes for Cu^+ effectively at both low and high Bcs concentrations (Figure 6b, trace ii, and Figure 6c, trace ii). Application of eq 10 to the experimental data (see Table S7A,B of the Supporting Information) confirmed that each protein domain binds Cu^I with high affinity in the subfemtomolar range. The K_D values of the four MBDs increase in the following order (i.e., their affinities for Cu^I decrease in that order):

$$\text{HMA7n}\ (10^{-18.2}\ \text{M}) < \text{HMA7/4n}\ (10^{-17.2}\ \text{M}) < \text{HMA2n} \sim \text{HMA4n}\ (10^{-16.6}\ \text{M}) \quad (11)$$

Each domain binds Cu^I more strongly than they bind Zn^{II} by a factor of $>10^6$ (Table 2). This is in odd contrast to a previous report (*13*) that HMA2n bound Cu^I more weakly (K_D = 13 μM) than Zn^{II} (K_D = 0.18 μM), and this issue is addressed further below. The K_D of ~13 μM for binding of Cu(I) to HMA2n reported previously (*13*) is meaningless, since no competing ligand was employed. Consequently, the apparent K_D value derived is close to the protein concentration employed in the experiment.

Confirmation of the Relative Binding Affinities for Cu^I and Zn^{II}. The competition experiments described above are subject to error in the reported formation constants of the ligand probes. This may render invalid comparisons such as those made above. For confirmation of the relative affinities, experiments were designed to allow Cu^+ and Zn^{2+} to compete for HMA2n and HMA4n under different conditions. In one series of experiments, excess free Cu^+ and Zn^{2+} (2 equiv each) competed directly for the MBDs and unbound metal ions were removed by a desalting column in the anaerobic glovebox. Metal analysis detected bound Cu^I only, supporting the previous conclusions that Cu^I and Zn^{II} bind competitively at a protein site(s) involving the same two Cys residues but that the affinity for Cu^I is much higher.

In a second series of experiments, Cu^I bound in $[Cu^I(Bca)_2]^{3-}$ was allowed to compete with free Zn^{2+} for HMA4n. Taking note of the experiments detailed in Figure 5, 1 and 2 equiv of Cu^+ were added to separate solutions of apo-HMA4n (10 μM) containing the Cu^I indicator Bca (45 μM). HMA4n bound 1 equiv of Cu^+ with high affinity, and the second equivalent of Cu^+ was trapped by Bca as $[Cu^I(Bca)_2]^{3-}$ quantitatively (cf. Figure 5). Further addition of 2 equiv of Zn^{2+} into each solution did not perturb the spectra, demonstrating that reaction 12 did not occur under the conditions:

$$Cu^I\text{−HMA4n} + Zn^{2+} + 2Bca^{2-} \not\rightarrow Zn^{II}\text{−HMA4n} + [Cu^I(Bca)_2]^{3-} \quad (12)$$

The result was verified by a separate experiment. Titration of Zn^{2+} into a solution containing Mf2 and Bca in a 1:2 molar ratio produced a plot indistinguishable from that of Figure 3b, trace i, indicating that Zn^{2+} is not trapped by Bca. On the other hand, when apo-HMA4n (10 μM) containing Bca (45 μM) was preloaded with 2 equiv of Zn^{2+} followed by 2 equiv of Cu^+, the experimental spectrum was indistinguishable from that of Figure 5, trace ii, indicating that back reaction 12 proceeds quantitatively. These results confirm the conclusions derived from the respective ligand competition experiments (Figures 3, 4, and 6): all four protein domains have much higher affinities for Cu^I than for Zn^{II} (Table 2).

Molecular Structure of Zn^{II}−HMA7n. The high-resolution X-ray crystal structure of zinc bound to copper-transporting domain HMA7n reveals a ferrodoxin-like scaffold with the MBM CxxC motif located on the first turn of α1 (Figure 7a and Table 3). The $\beta\alpha\beta\beta\alpha\beta$ topology places HMA7n in the same structural fold family as Atox1, a Cu^I metallochaperone (Figure 7b; Protein Data Bank entry 1FEE) (*25*). Superposition of the entire Cα traces of Zn^{II}−HMA7n and Atox1 reveals differences that are subtle and mainly restricted to loop regions connecting secondary structural elements. In particular, Zn^{II}−HMA7n is marked by a three-residue insertion into the β3−α2 loop, and one extra residue in the α1−β2 connector.

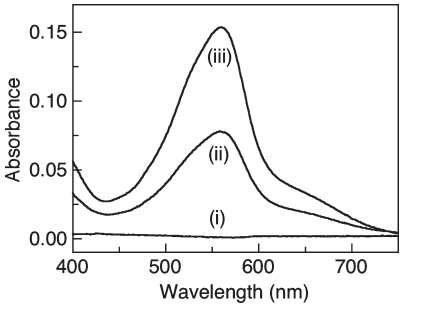

FIGURE 5: Solution spectra of a mixture of apo-HMA4n (10 μM) and Bca (45 μM) in 50 mM Mops buffer (pH 7.3) with 100 mM NaCl upon addition of (i) 10 μM Cu^+ or (ii) 20 μM Cu^+. (iii) Same as trace ii but without HMA4n. Spectra were not affected when the concentration of Bca was doubled to 90 μM or by addition of Zn^{2+} (20 μM) either before or after the addition of Cu^+.

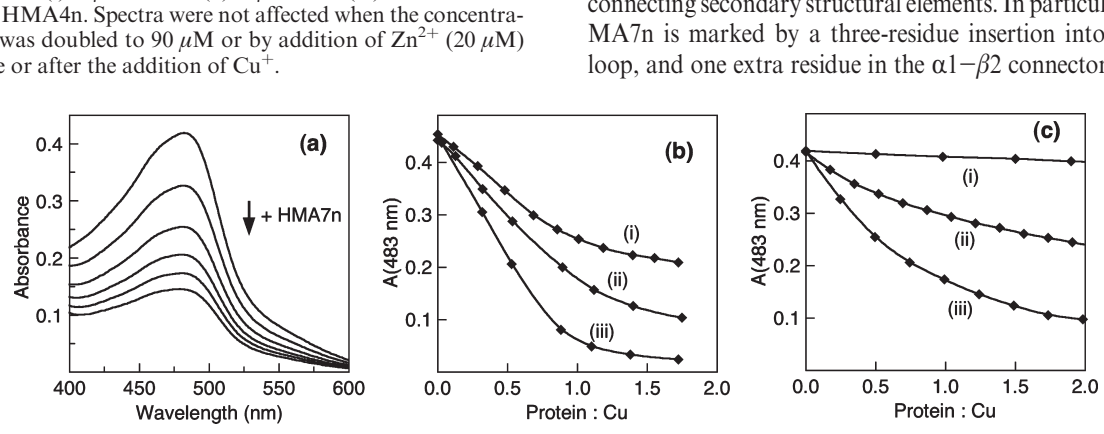

FIGURE 6: Determination of Cu^I dissociation constants (K_D) for HMA2n, HMA4n, and HMA7n proteins in 50 mM Mops buffer (pH 7.3) with 100 mM NaCl with the probe Bcs. (a) Changes in the solution spectrum of a mixture containing Cu^I (30 μM) and Bcs (500 μM) in the presence of increasing HMA7n concentrations (0, 15, 30, 60, 88, and 175 μM). (b and c) Variation of A_{483} {proportional to $[Cu^I(Bcs)_2{}^{3-}]$} with the P:Cu ratio: (i) HMA4n (or HMA2n), (ii) HMA7/4n chimera, and (iii) HMA7n. In panel b, $[Cu^I]_{total} \sim 35$ μM and $[Bcs]_{total}$ = 200 μM; in panel c, $[Cu^I]_{total}$ = 32 μM and $[Bcs]_{total}$ = 500 μM.

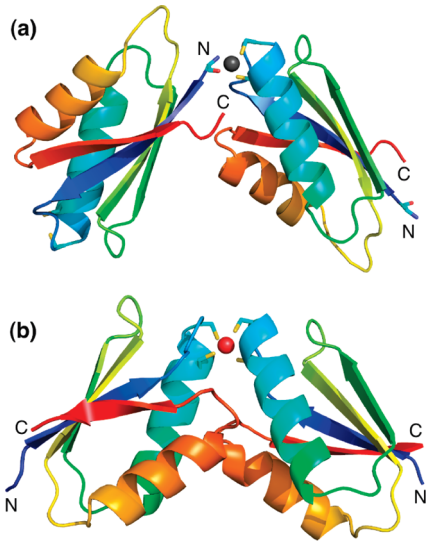

FIGURE 7: Comparison of crystal structures of (a) $(Zn^{II}-HMA7n)_m$ and (b) $Cu^{I}-(Atox1)_2$ (Protein Data Bank entry 1FEE). The structures are represented as Cα traces with secondary structure indicated. The chains are colored from blue at the N-terminus to red at the C-terminus. The Zn^{II} and Cu^{I} atoms are shown as gray and red spheres, respectively. The metal ligands are shown as sticks.

Although the affinity of HMA7 for Zn^{2+} is much lower than its affinity for Cu^{+}, the copper-bound form failed to crystallize under reducing but aerobic conditions. Coordination of the Zn^{2+} ion by adjacent HMA7n molecules links them into a chain parallel to the *z*-axis of the crystal lattice. In the chain, each Zn^{II} ion occupies a distorted tetrahedral site formed from two Cys ligands from the CxxC motif of one HMA7n molecule and the amino N and carbonyl O atoms of the N-terminal methionine of another. Metal−ligand bonding distances are as follows: ^{Cys13}S−Zn, 2.24 Å; ^{Cys16}S−Zn, 2.23 Å; ^{Met1}N−Zn, 2.17 Å; and ^{Met1}O−Zn, 2.22 Å. The S−Zn−S angle is 128.2°, and the O−Zn−N angle is 78.7°. The coordinates of $Zn^{II}-HMA7n$ have been deposited in the Protein Data Bank as entry 3DXS.

Interestingly, the crystal structures of M−Atox1 species (M = Cu^{I}, Hg^{II}, or Cd^{II}) reveal a symmetric dimer linked by the metal ion (Figure 7b) (*25*). The Cd^{II} ion is ligated by four Cys residues from two CxxC motifs of the two monomers in a tetrahedral geometry, while Cu^{I} and Hg^{II} are coordinated by two Cys residues from one monomer and one Cys only from the second. These arrangements have been used as a structural basis for models of Cu^{I} transfer between proteins. The metal complex is stabilized by metal bonding and an extended hydrogen bonding network around the metal-binding site (*25*).

Solution Structure of $Zn^{II}-HMA4n$. Zinc-transporting domain HMA4n (residues 2−96) was isotopically labeled and the solution structure of the Zn^{II}-loaded form determined using NMR. Resonance assignments were made with a standard array of multidimensional NMR techniques (*26*). Backbone assignments were complete for residues 7−92, and only residues 3 and 93 have no assignments. Partial assignments were obtained for other resonances. Side chain assignments were essentially complete over residues 13−89. Backbone resonance assignments for apo-HMA4 were incomplete, with amide resonance assignments missing for residues 1−4, 6, 27−30, 87, and 90−96 (Figure 8).

The solution structure of Zn−HMA4n was calculated using CYANA (*27*) and refined using Xplor-NIH (*28*, *29*). The structure consists of a ferredoxin βαββαβ fold with strands β1 (residues 17−23), helix α1 (residues 32−41), strand β2 (residues

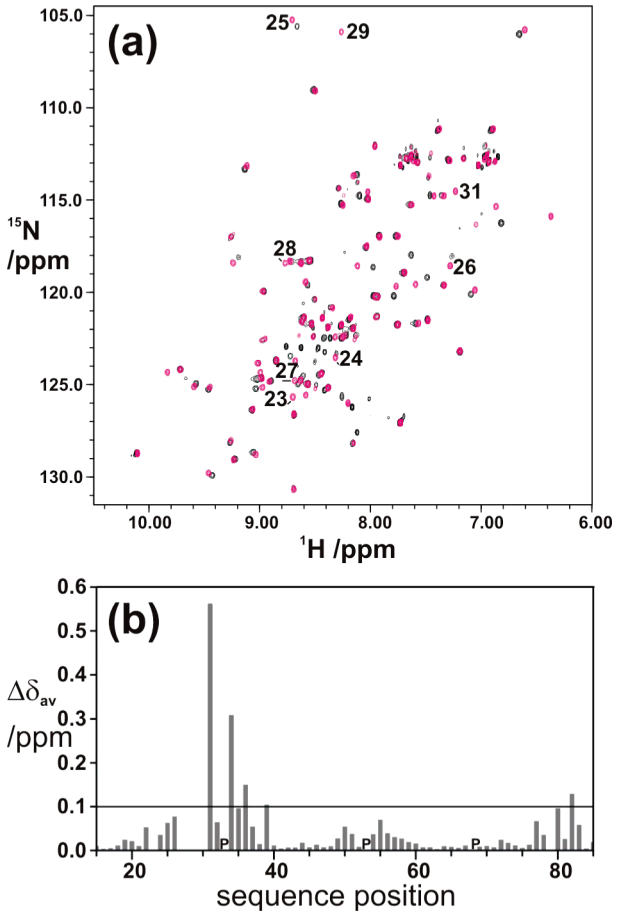

FIGURE 8: (a) Overlaid $^{1}H-^{15}N$ HSQC spectra of apo-HMA4n (black) and $Zn^{II}-HMA4n$ (pink) in 50 mM KP_i buffer (pH 6.7) with 5% D_2O. The protein concentrations are in the range of 0.5−1.0 mM. Resonances in the β1−α1 loop are labeled for $Zn^{II}-HMA4$. (b) Weighted-average chemical shift differences of amide resonances $\{\Delta\delta_{av}(HN) = [(\Delta\delta_H^2 + \Delta\delta_N^2/25)/2]^{1/2}\}$ between apo and Zn^{II}-bound HMA4n. Only $\Delta\delta_{av}$ values for residues 15−85, encompassing the structured region, are shown. The differences for those residues with proline (indicated by P) or missing amide assignments (residues 23 and 27−30) are set to $\Delta\delta_{av} = 0$ ppm.

45−51), β3 (residues 56−61), α2 (residues 68−77), and β4 (residues 82−84). The N- and C-terminal tails have no long-range structure (residues 2−15 and 86−96, respectively) (Figure 9a). The core residues of HMA4n are well-ordered with pairwise rmsd values over the residues in the ordered secondary structure of 0.36 ± 0.09 Å and over all heavy atoms of the same residues of 1.05 ± 0.12 Å. The structural statistics are summarized in Table 4, and the coordinates have been deposited in the Protein Data Bank as entry 2KKH.

A metal-binding site is formed by the ICCTSE sequence located in the β1−α1 loop. The structure brings glutamic acid residue E31 into the proximity of adjacent Cys residues C27 and C28 (Figure 9a). Conserved E31 immediately precedes the start of α1, and the side chain projects toward the two cysteines (Figures 9a and 11a). NOEs are observed between the side chain resonances of E31 and the amides of C27 and C28 that would be predicted if the γ-carboxylate of E31 is bound to Zn in a tetrahedral site. Specifically, strong NOEs are observed between E31 Hβ protons and the amide of C27 and weak NOEs between the amide of C28 and side chain E31 resonances. In addition, strong NOEs are observed between the side chains of I26 and E31. The presence of these NOEs indicates the proximity of those

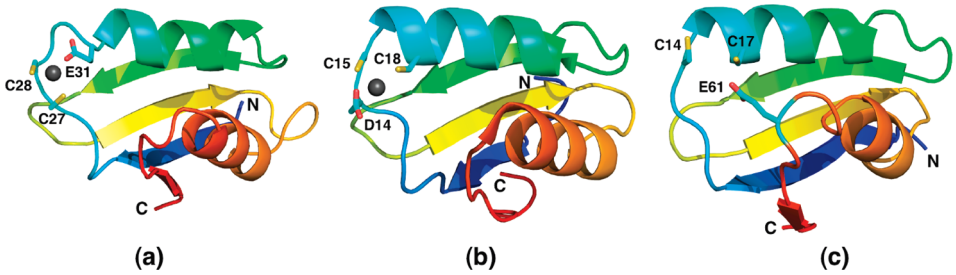

FIGURE 9: Comparison of NMR structures: (a) Zn−HMA4n, (b) Zn−ZntAn (Protein Data Bank entry 1MWZ), and (c) apo-CadAn (Protein Data Bank entry 2AJ1). The structures are represented as Cα traces with secondary structure indicated. The chains are colored from blue at the N-terminus to red at the C-terminus. The Zn atoms are shown as gray spheres with the metal ligands as sticks.

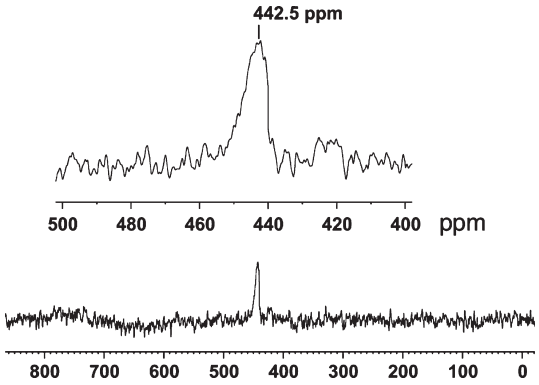

FIGURE 10: ^{113}Cd NMR spectrum of Cd^{II}−HMA4n (0.5 mM) in KP_i (50 mM, pH 7.3) at 110 MHz and 25 °C. The chemical shift is plotted relative to that of 0.1 M $Cd(ClO_4)_2$ (δ = 0 ppm). Observation of a single resonance at 442.5 ppm is consistent with the presence of a CdS_2OX center (X = O or N).

residues in the metal-binding site. In addition, the residues in this region experience the largest perturbation of their amide resonance chemical shifts upon addition of Zn^{2+}, while resonances in other region are largely unaffected (Figure 8).

Further support is provided by the ^{113}Cd NMR experiments. A single resonance centered at 442.5 ppm was detected in the ^{113}Cd NMR spectrum of a ^{113}Cd-loaded HMA4n sample (Figure 10). The ^{113}Cd chemical shift is highly sensitive to the coordination environment of the metal ion and varies more than 1000 ppm with different environments and, in particular, with the number of thiolate ligands: the more thiolate ligands, the further downfield the ^{113}Cd resonance occurs (*30*). The ^{113}Cd chemical shift of Cd−HMA4n is consistent with Cd^{II} bound to no more than two thiolate ligands. A Cys_2 motif in Cd-substituted tyrosine kinases resonates in the vicinity of 460 ppm (*31*), close to that of 442.5 ppm observed in Cd−HMA4n. In contrast, ^{113}Cd-loaded CadA resonates at 687 ppm, indicative of a Cys_3 supporting a CdS_3O center (*32*). The results suggest that the Zn^{II} ion in Zn−HMA4n is coordinated by the side chains of C27 and C28. In addition, the sequence conservation (Figure 11) and proximity of E31 to these cysteine residues suggested that it was a Zn ligand. Consequently, a zinc ion was modeled into a tetrahedral site formed by C27, C28, and E31 (carboxylate) with a water molecule in the absence of any suitable nearby fourth ligand from the protein. Structures were first calculated in the absence of the metal, and no violations of experimental constraints were observed upon addition of a Zn center.

DISCUSSION

Metal Probes. Metal selectivity in biology is complex and poorly understood in detail, but it seems that a combination of thermodynamics (affinity), kinetics (including protein−protein interactions), and compartmentalization is operating (*33*−*35*). Different mechanisms are employed to ensure insertion of the appropriate metal into the appropriate location.

Reliable evaluation and comparison of metal binding affinities is important for a more detailed understanding of metal selection and speciation. However, estimation of these metal binding constants may be said to be in some disarray because of disparate values reported in the literature. A few examples serve to illustrate the problem.

(1) The prion protein can bind multiple Cu^{2+} ions in versatile sites of the so-called octa-repeat region. Reported K_D values range from 10^{-6} to 10^{-9} M, with one estimate of 10^{-14} M (*36*−*39*).

(2) Estimated K_D values for binding of Cu^{2+} to the amyloid-β peptide range from 10^{-6} to 10^{-10} M, with one estimate of 10^{-18} M (*40*).

(3) Reported K_D values for the Cu^I metallochaperone Atox1 differ by more than 10 orders of magnitude (*24*, *41*−*43*).

(4) Reported K_D values for the binding of Co^{2+} to the N-terminal zinc-binding peptide of the HIV-1 nucleocapsid protein vary by 6 orders of magnitude (10^{-6}−10^{-12} M) (*44*).

A synthetic ligand can provide a reliable probe for estimation of metal binding affinities (dissociation constants, K_D) if an effective competition can be induced between the protein and the ligand for the metal ion and if the essential concentrations can be quantified. In this work, the challenges of employing four of the most popular chromophoric probes for Cu^+ and Zn^{2+} were evaluated and applied to the N-terminal MBDs of selected HMA P_{1B}-type ATPases of *A. thaliana*. The relative affinities were verified by independent cross-checks. An important aspect for the MBMs examined here was to confirm via the Ellman assay that the Cys residues were in their reduced thiol forms and to maintain that redox state by working under anaerobic reducing conditions. Oxidation to disulfide links compromises the estimations of K_D.

Mf2 is a sensitive spectroscopic probe for many divalent cations, including Zn^{2+}, and has been used to estimate the Zn^{II} binding affinities of a number of proteins (*13*, *19*, *45*, *46*). However, quantitative estimation is often hindered by its narrow metal buffering range that is imposed by an experimental detection limit on total Mf2 concentration of ~35 μM due to the fact that the probe detects Zn^{II} binding indirectly via the absorbance of the free ligand (see Figure S2 of the Supporting Information). In this work, Mf2 was suitable as a quantitative probe for HMA7n and the HMA7/4n chimera, but not for HMA2n and HMA4n.

The bidentate ligand Par is another popular Zn^{2+} probe and has the advantage of a much wider Zn^{2+} buffering range (Figure S2 of the Supporting Information). Consequently, it is capable of

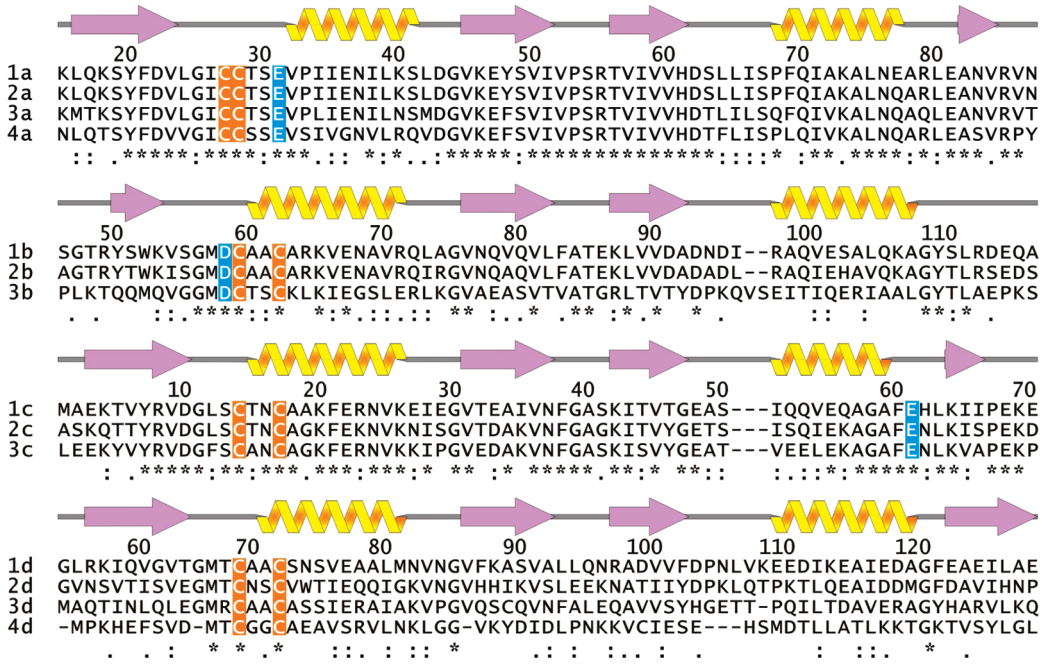

FIGURE 11: Structure and sequence alignments of the N-terminal metal-binding domains of P_{1B}-type ATPases. Group a consists of HMA-type Zn transporter domains HMA4n (1a, AAL84162), HMA2n (3a, AAR10767), HMA3n from *A. thaliana* (4a, AAL16382), and HMA4n from *A. halleri* (2a, AAY29151). Group b consists of ZntA-type Zn transporter domains ZntAn from *E. coli* (1b, NP_414542) and from *Salmonella typhimurium* (2b, Q8ZLE5) and ZiaAn from *Synechocystis* PCC 6803 (3b, NP_442636). Group c consists of CadA-type Cd transporter domains CadAn from *Listeria monocytogenes* (1c, Q60048), *Streptococcus thermophilus* (2c, CAE52410), and *Staphylococcus epidermidis* ATCC 12228 (3c, AAO03672). Group d consists of Atox1-type Cu transporters or transporter domains HMA7n from *A. thaliana* (1d, the first N-terminal MBD, NP_199292), ATP7An1 from *Homo sapiens* (2d, the first N-terminal MBD, CAA49145), PacSn from *Synechocystis* PCC 6803 (3d, NP_440588), and Atox1 from *H. sapiens* (4d, NP_004036). The secondary structure elements and residue numbering shown at the top of each group of proteins are derived from NMR or X-ray crystal structures and the original protein sequence of the first protein member in each group: HMA4n (1a, this work), ZntAn (1b, Protein Data Bank entry 1MWZ), CadAn (1c, Protein Data Bank entry 2AJ1), and HMA7n (1d, this work). The conserved residues proposed to be involved in divalent cation binding in groups a−c and in Cu^I binding in group d are highlighted.

quantitatively defining K_D values for a wider range of affinities. However, both the molar absorptivity (ε) and formation constant (β_2) of "$Zn(Par)_2$" are sensitive to pH and vary markedly within the important buffer range of pH 7−9 (Table S5 of the Supporting Information). This prevents quantitative estimation of Zn^{II} binding affinities of proteins by the use of the Par probe alone, but nevertheless, it has been applied widely (*19*−*22*, *47*). This restriction can be overcome by use of a spectroscopically silent ligand of known and appropriate affinity in calibrating the affinity of Par for Zn^{II} under the relevant experimental conditions (Figure 4 and Table 2). The ligand Egta was employed here.

The affinity of each apoprotein for Cu^I was estimated with two Cu^I-specific ligands, Bca and Bcs, as described previously (*23*, *24*). Like the Par probe for Zn^{II}, these ligands form 1:2 metal complexes, $[Cu^I(Bca)_2]^{3-}$ and $[Cu^I(Bcs)_2]^{3-}$, respectively, with detection of Cu^I binding based on the complexes rather than on the free ligands. This feature, and the difference in the formation constants of the two complexes ($\beta_2 = 10^{17.2}$ and $10^{19.8}$, respectively),[2] allows Cu^I binding affinities of different proteins to be estimated reliably within a wide K_D range of 10^{-11}−10^{-19} M (*23*, *24*, *48*−*51*). The relative Cu^I binding affinities estimated via these two probes can be cross-checked and verified by independent direct Cu^I-exchange reactions between different proteins (*24*, *48*, *50*, *51*). The ligand Bca was unable to compete for the first equivalent of Cu^I with each of the four HMA protein domains, demonstrating their high Cu^I binding affinities. Consequently, their affinities were estimated quantitatively with the stronger Cu^I ligand, Bcs (Figure 6 and Table 2).

Metal Binding Affinities and Molecular Structures. The HMA2n domain (including residues 1−75 with a C-terminal Strep tag) was expressed and isolated recently (*13*). Since the C-terminus of a ferredoxin fold protein is distant from the expected metal-binding site (see Figures 7 and 9), the HMA2n domain of residues 1−79 (without a tag) studied in this work is expected to have similar metal binding properties. The Zn^{II} binding affinity estimated for HMA2n(1−75+tag) was similar to that of Mf2 at pH 7 ($K_D \sim 10^{-8}$ M), in reasonable agreement with the estimates at pH 7.3 ($K_D < 10^{-9}$ M) obtained with Mf2 in this study for both HMA2n(1−79) and HMA4n (Table 2). However, the estimate for K_D of $\sim 10^{-5}$ M for Cu^I binding to HMA2n(1−75+tag) is in sharp contrast to the present estimates on the subfemtomolar level for HMA2n(1−79) and HMA4n (Table 2). To clarify the situation, experiments involving direct competition for HMA2n (or HMA4n) between Zn^{2+} and Cu^+ and between Zn^{2+} and $[Cu^I(Bca)_2]^{3-}$ were conducted, and the results demonstrated that the affinities of both Zn transporter domains HMA2n and HMA4n for Cu^I are indeed much higher than those for Zn^{II} (Figure 5).

The classic MBM CxxC motif within the $\beta\alpha\beta\beta\alpha\beta$ ferredoxin fold usually exhibits exceptionally high affinity (subfemtomolar level) for Cu^I (*24*, *49*). The MTCAAC motif of HMA7n and the equivalent ICCTSE motif of HMA2n and HMA4n also exhibit high affinities for Cu^I (Table 2). Cu^I binding blocked detection of

[2]A smaller β_2 of 4.6×10^{14} M^{-2} for $[Cu^I(Bca)_2]^{3-}$ was estimated independently by isothermal titration calorimetry (*41*). In that work, the Cu^+ solution was generated by reduction of Cu^{2+} with ascorbate in 200 mM NaCl which stabilizes Cu^+ as $[Cu^ICl_4]^{3-}$ and related chloro complexes. Titration with Bca would involve a conversion of species such as $[Cu^ICl_4]^{3-}$ (rather than Cu^+_{aq}) to $[Cu^I(Bca)_2]^{3-}$, diminishing the observed heat release.

both cysteinyl thiols, completely consistent with both residues in each MBM being bound to Cu^{I}. This is at variance with a previous suggestion that only one of the two Cys residues in HMA2n was a ligand (*13*). The ICCTSE motif can bind a second equivalent of Cu^{I} with lower affinity, and this appears to be one of its characteristics. For example, HMA7n binds 1 equiv of Cu^{I} only while chimera HMA7/4n (which contains the ICCTSE motif) can bind 2 equiv of Cu^{I} (Table 1).

The CxxC motif in copper transporting protein HMA7n also binds Zn^{II} with nanomolar affinity. Gel-filtration analysis revealed essentially identical elution profiles for both the apo and Zn^{II} forms with an elution volume consistent with the presence of monomeric forms in solution (Figure S1 of the Supporting Information). This indicates that the Zn^{II} ion is coordinated within a single HMA7n molecule. Both Cys residues were confirmed to be involved in the Zn^{II} binding, and the two remaining coordination sites were presumably derived from solvent or buffer. However, the crystal structure of Zn^{II}−HMA7n revealed a polymeric chain [$(Zn^{II}$−HMA7n$)_m$] in which each Zn^{II} ion bridged two adjacent HMA7n molecules via coordination to two Cys residues from the CxxC motif on one molecule and the amino N and O atoms of the N-terminal methionine on the other (Figure 7a). It is likely that the high protein concentrations in the crystals (~70 mM) led to substitution of the metal ligands derived from solvent or buffer present in solution.

Thiol assays indicated that both Cys residues in the CCTSE motif were Zn^{II} ligands in zinc transporting domains HMA2n and HMA4n, consistent with previous mutagenesis analysis of HMA2n (*13*). That analysis suggested further that the E31 residue in the CCTSE motif was another Zn^{II} ligand (*13*). This interpretation is supported by the structure of Zn^{II}−HMA4n determined in this work. The E31 residue is in the proximity of the two Cys residues and is conserved among plant Zn^{2+}−HMA homologues (Figures 9a and 11a). The ^{113}Cd chemical shift of a Cd−HMA4n sample is consistent with a $Cd^{II}S_2OX$ (X = O or N) site. Two other distinct groups of P_{1B}-type ATPases responsible for divalent cation transportation, ZntA and CadA, also contain MBDs and MBMs similar in structure (Figures 9 and 11) (*14*, *32*). The two Cys residues in the $\beta1-\alpha1$ loop are metal ligands in each case, but the positions in the primary structure of the putative carboxylate ligands are different. In ZntA, the carboxylate ligand is provided by D58, a residue in the $\beta1-\alpha1$ loop immediately preceding the two Cys residues in the DCxxC motif (Figures 9b and 11b). In CadA, the carboxylate ligand is contributed by distant residue E61 in the $\alpha2-\beta4$ loop (Figures 9c and 11c). These carboxylate residues appear to play a role in fine-tuning the binding affinity and specificity for the divalent cations. Consistent with this model, introduction of the MBM ICCTSE motif of HMA4n into the equivalent position in HMA7n decreased its affinity for Zn^{II} by a factor of 100 (Table 2). This is likely caused by structural perturbation of the Glu residue in the new protein environment. On the other hand, mutation of this Glu residue to either Cys or Ala in HMA2n abolished its Zn^{II} binding completely (*13*).

Metal Selectivity. HMA2 and HMA4 are required for zinc homeostasis in *A. thaliana*, and the N-terminal domain of HMA2 (and likely HMA4 as well) is essential for function (*6*, *9*). Experimental data based on both the Mf2 and Par probes demonstrate that HMA2n and HMA4n bind Zn^{II} with similar affinities in the subnanomolar range ($K_D \sim 10^{-10}$ M), higher than that of HMA7n by a factor of 20−30 (Figures 3 and 4 and Table 2). The Bcs probe demonstrates that the affinities of HMA2n and HMA4n for the first equivalent of Cu^{I} are also similar but are lower than that of HMA7n by a factor of 30−50 (Figure 6 and Table 2). These values are consistent with the respective roles of HMA2n, HMA4n, and HMA7n in Zn^{2+} and Cu^{+} transportation. However, each of the four MBDs has a much higher affinity for Cu^{I} than each has for Zn^{II}: $K_D(Cu^{I})/K_D(Zn^{II}) < 10^{-6}$ (Table 2). If both metal ions were equally available, each MBD would select Cu^{I} only. How do HMA2 and HMA4 select for Zn^{II}?

The cyanobacterium *Synechocystis* PCC 6803 contains several metal transporters, including ZiaA for Zn and PacS for Cu as well as a cytosolic copper chaperone Atx1. Both ZiaA and PacS are P1-type ATPases with similar ferredoxin-type N-terminal MBDs ZiaAn and PacSn (sequences 3b and 3d, respectively, in Figure 11), respectively. However, consistent with this study of HMA MBDs, domain ZiaAn of Zn transporter ZiaA was found to bind Cu^{+} more strongly than Zn^{2+} (*52*). Metal selection of ZiaA for zinc appeared to be under kinetic control as a bacterial two-hybrid assay detected direct interaction of the copper-delivering chaperone Atx1 with PacSn, but not with the equivalent ZiaAn (*52*). Provided that there is no free copper available in the cytoplasm of *Synechocystis* PCC 6803, programmed incompatibility between ZiaAn and Atx1 would deny ZiaA access to copper. On the other hand, thermodynamic preferences based on relative affinities may also operate to enhance metal selectivity, and a quantitative comparison of the binding affinities of ZiaAn and PacSn for Cu^{I} and Zn^{II} would be interesting.

A copper chaperone AtCCH1 has been identified in *A. thaliana* (*53*). It is not known yet if preferential protein−protein interactions ensure delivery of copper to HMA7, but not to HMA2 or HMA4. In this work, we show that thermodynamic considerations favor such speciation.

(i) The affinity for Cu^{I} of the domain HMA7n from copper transporter HMA7 is 30−50 times higher than that of HMA4n from zinc transporter HMA4. Binding of Cu^{I} to HMA7 is favored. This selectivity appears to be induced by the low coordination number demanded by Cu^{+} and the optimal positioning of two ligands only in the CysxxCys motif.

(ii) The affinity for Zn^{II} of HMA4n from zinc transporter HMA4 is 20−30 times higher than that of HMA7n from copper transporter HMA7. Binding of Zn^{II} to HMA4 is favored. This selectivity appears to be induced by the presence of the anionic ligand Glu in addition to the two Cys ligands in the CysCysxxGlu motif.

(iii) The affinities for Cu^{I} of HMA4n and HMA7n are at least 6 orders of magnitude higher than their affinities for Zn^{II}: $K_D(Cu^{I})/K_D(Zn^{II}) < 10^{-6}$. The fine-tuning present in scenarios (i) and (ii) cannot overcome the thermodynamic effect of the presence of two Cys ligands. Selection of Zn^{II} by HMA4 under metal limiting conditions must be ensured by the presence of high-affinity Cu^{I} binding proteins that bind Cu^{I} very tightly and by kinetics (including protein−protein interactions) and/or compartmentalization (*33*−*35*).

These conclusions emphasize the toxicity of free Cu^{+} arising from its redox activity and its high affinity for thiol ligands. It also rationalizes the fact that the various copper sensor proteins operate normally at sensitivities (10^{-17}−10^{-20} M) that are ~6 orders of magnitude lower than those for zinc sensors (10^{-11}−10^{-14} M) (*54*).

In conclusion, cells employ multiple strategies to control metal transportation and speciation. The thermodynamic constraints

are supported by evolved kinetic imperatives such as favorable molecular interactions between partner proteins like those observed in the ZiaA−PacS−Atx1 system discussed above. In addition, cell compartmentalization is another strategy for overcoming large thermodynamic barriers to correct metal selection (*34*). However, thermodynamic gradients operate at different stages to drive the process of metal transportation. Here we show that subtle variations in the metal-binding site and protein environment in a common ferredoxin-type scaffold can modulate the relative metal binding affinities of similar proteins.

ACKNOWLEDGMENT

We thank Dr. Terry Mulhern for his help with initial NMR data collection and analysis and Mr. Chak Ming Sze for assistance with ESI-MS experiments. J.G. thanks Clemens Shulze-Briese and beamline scientists at the Swiss Light Source (SLS), the Australian Synchrotron Research Program for airfares to SLS, and Marc Kvansakul for technical assistance at WEHI. NMR data were acquired at the Bio21 Institute NMR facility, the University of Melbourne.

SUPPORTING INFORMATION AVAILABLE

PCR primers, ESI-MS data, calculation of conditional binding constants, solution characters of Zn(II) probes, estimation of protein metal binding affinities, gel-filtration elution profile, and analysis of the metal buffer range (Tables S1−S7) and full structure solution and refinement of Zn−HMA7 (Figures S1 and S2). This material is available free of charge via the Internet at http://pubs.acs.org.

REFERENCES

1. Lutsenko, S., and Petris, M. J. (2003) Function and Regulation of the Mammalian Copper-transporting ATPases: Insights from Biochemical and Cell Biological Approaches. *J. Membr. Biol. 191*, 1–12.
2. Williams, L. E., and Mills, R. F. (2005) P1B-ATPases: An ancient family of transition metal pumps with diverse functions in plants. *Trends Plant Sci. 10*, 491–502.
3. Argüello, J. M. (2003) IIdentification of Ion-Selectivity Determinants in Heavy-Metal Transport P1B-type ATPases. *J. Membr. Biol. 195*, 93–108.
4. Axelsen, K. B., and Palmgren, M. G. (2001) Inventory of the Superfamily of P-Type Ion Pumps in *Arabidopsis*. *Plant Physiol. 126*, 696–706.
5. Sinclair, S. A., Sherson, S. M., Jarvis, R., Camakaris, J., and Cobbett, C. S. (2007) The use of the zinc-fluorophore, Zinpyr-1, in the study of zinc homeostasis in *Arabidopsis* roots. *New Phytol. 174*, 39–45.
6. Hussain, D., Haydon, M. J., Wang, Y., Wong, E., Sherson, S. M., Young, J., Camakaris, J., Harper, J. F., and Cobbett, C. S. (2004) P-Type ATPase Heavy Metal Transporters with Roles in Essential Zinc Homeostasis in *Arabidopsis*. *Plant Cell 16*, 1327–1329.
7. Hanikenne, M., Talke, I. N., Haydon, M. J., Lanz, C., Nolte, A., Motte, P., Kroymann, J., Weigel, D., and Kramer, U. (2008) Evolution of metal hyperaccumulation required cis-regulatory changes and triplication of HMA4. *Nature 453*, 391–395.
8. Verret, F., Gravot, A., Auroy, P., Preveral, S., Forestier, C., Vavasseur, A., and Richaud, P. (2005) Heavy metal transport by AtHMA4 involves the N-terminal degenerated metal binding domain and the C-terminal His11 stretch. *FEBS Lett. 579*, 1515–1522.
9. Wong, C. K. E., Jarvis, R. S., Sherson, S. M., and Cobbett, C. S. (2009) Functional analysis of the heavy metal binding domains of the Zn/Cd-transporting ATPase, HMA2, in *Arabidopsis thaliana*. *New Phytol. 181*, 79–88.
10. Mills, R. F., Francini, A., Ferreira da Rocha, P. S. C., Baccarini, P. J., Aylett, M., Krijger, G. C., and Williams, L. E. (2005) The plant P1B-type ATPase AtHMA4 transports Zn and Cd and plays a role in detoxification of transition metals supplied at elevated levels. *FEBS Lett. 579*, 783–791.
11. Burkhead, J. L., Reynolds, K. A., Abdel-Ghany, S. E., Cohu, C. M., and Pilon, M. (2009) Copper homeostasis. *New Phytol. 182*, 799–816.
12. Woeste, K. E., and Kieber, J. J. (2000) A Strong Loss-of-Function Mutation in RAN1 Results in Constitutive Activation of the Ethylene Response Pathway as Well as a Rosette-Lethal Phenotype. *Plant Cell 12*, 443–455.
13. Eren, E., Gonzalez-Guerrero, M., Kaufman, B. M., and Arguello, J. M. (2007) Novel Zn^{2+} coordination by the regulatory N-terminus metal binding domain of *Arabidopsis thaliana* Zn^{2+}-ATPase HMA2. *Biochemistry 46*, 7754–7764.
14. Banci, L., Bertini, I., Ciofi-Baffoni, S., Finney, L. A., Outten, C. E., and O'Halloran, T. V. (2002) A new zinc-protein coordination site in intracellular metal trafficking: Solution structure of the Apo and Zn(II) forms of ZntA(46−118). *J. Mol. Biol. 323*, 883–897.
15. Zimmermann, M., Xiao, Z., Cobbett, C. S., and Wedd, A. G. (2009) Metal specificities of *Arabidopsis* zinc and copper transport proteins match the relative, but not the absolute, affinities of their N-terminal domain. *Chem. Commun.*, 6364–6366.
16. Simons, T. J. B. (1993) Measurement of free Zn^{2+} ion concentration with the fluorescent probe mag-fura-2 (furaptra). *J. Biochem. Biophys. Methods 27*, 25–37.
17. Corsini, A., Fernando, Q., and Freiser, H. (1963) The Effect of Metal Ion Chelation on the Acid Dissociation of the Ligand 4-(2-Pyridylazo)-resorcinol. *Inorg. Chem. 2*, 224–226.
18. Tanaka, M., Funahashi, S., and Shirai, K. (1968) Kinetics of the Ligand Substitution Reaction of the Zinc 4-(2-Pyridylazo)resorcinol Complex with (Ethylene glycol)bis(2-aminoethyl ether)-N,N,N′,N′-tetraacetic Acid. *Inorg. Chem. 7*, 573–578.
19. Liu, J., Stemmler, A. J., Fatima, J., and Mitra, B. (2005) Metal-binding characteristics of the amino-terminal domain of ZntA: Binding of lead is different compared to cadmium and zinc. *Biochemistry 44*, 5159–5167.
20. Dinkova-Kostova, A. T., Holtzclaw, W. D., and Wakabayashi, N. (2005) Keap1, the sensor for electrophiles and oxidants that regulates the phase 2 response, is a zinc metalloprotein. *Biochemistry 44*, 6889–6899.
21. VanZile, M. L., Cosper, N. J., Scott, R. A., and Giedroc, D. P. (2000) The zinc metalloregulatory protein *Synechococcus* PCC7942 SmtB binds a single zinc ion per monomer with high affinity in a tetrahedral coordination geometry. *Biochemistry 39*, 11818–11829.
22. Zhou, Z. S., Peariso, K., Penner-Hahn, J. E., and Matthews, R. G. (1999) Identification of the zinc ligands in cobalamin-independent methionine synthase (MetE) from *Escherichia coli*. *Biochemistry 38*, 15915–15926.
23. Xiao, Z., Donnelly, P. S., Zimmermann, M., and Wedd, A. G. (2008) Transfer of Copper between Bis(thiosemicarbazone) Ligands and Intracellular Copper-Binding Proteins. Insights into Mechanisms of Copper Uptake and Hypoxia Selectivity. *Inorg. Chem. 47*, 4338–4347.
24. Xiao, Z., Loughlin, F., George, G. N., Howlett, G. J., and Wedd, A. G. (2004) C-Terminal Domain of the Membrane Copper Transporter Ctr1 from *Saccharomyces cerevisiae* Binds Four Cu(I) Ions as a Cuprous-Thiolate Polynuclear Cluster: Sub-femtomolar Cu(I) Affinity of Three Proteins Involved in Copper Trafficking. *J. Am. Chem. Soc. 126*, 3081–3090.
25. Wernimont, A. K., Huffman, D. L., Lamb, A. L., O'Halloran, T. V., and Rosenzweig, A. C. (2000) Structural basis for copper transfer by the metallochaperone for the Menkes/Wilson disease proteins. *Nat. Struct. Biol. 7*, 766–771.
26. Sattler, M., Schleucher, J., and Griesinger, C. (1999) Heteronuclear multidimensional NMR experiments for the structure determination of proteins in solution employing pulsed field gradients. *Prog. Nucl. Magn. Reson. Spectrosc. 34*, 93–158.
27. Guntert, P. (2004) Automated NMR structure calculation with CYANA. *Methods Mol. Biol. 278*, 353–378.
28. Schwieters, C. D., Kuszewski, J. J., and Clore, G. M. (2006) Using Xplor-NIH for NMR molecular structure determination. *Prog. Nucl. Magn. Reson. Spectrosc. 48*, 47–62.
29. Schwieters, C. D., Kuszewski, J. J., Tjandra, N., and Clore, G. M. (2003) The Xplor-NIH NMR molecular structure determination package. *J. Magn. Reson. 160*, 65–73.
30. Hemmingsen, L., Olsen, L., Antony, J., and Sauer, S. P. A. (2004) First principle calculations of ^{113}Cd chemical shifts for proteins and model systems. *J. Biol. Inorg. Chem. 9*, 591–599.
31. Ahmadibeni, Y., Hanley, M., White, M., Ayrapetov, M., Lin, X., Sun, G., and Parang, K. (2007) Metal-binding properties of a dicysteine-containing motif in protein tyrosine kinases. *ChemBioChem 8*, 1592–1605.
32. Banci, L., Bertini, I., Ciofi-Baffoni, S., Su, X.-C., Miras, R., Bal, N., Mintz, E., Catty, P., Shokes, J. E., and Scott, R. A. (2006) Structural Basis for Metal Binding Specificity: The N-terminal Cadmium Binding Domain of the P1-type ATPase CadA. *J. Mol. Biol. 356*, 638–650.

33. Waldron, K. J., and Robinson, N. J. (2009) How do bacterial cells ensure that metalloproteins get the correct metal? *Nat. Rev. Microbiol. 7*, 25–35.
34. Tottey, S., Waldron, K. J., Firbank, S. J., Reale, B., Bessant, C., Sato, K., Cheek, T. R., Gray, J., Banfield, M. J., Dennison, C., and Robinson, N. J. (2008) Protein-folding location can regulate manganesebinding versus copper- or zinc-binding. *Nature 455*, 1138–1145.
35. Finney, L. A., and O'Halloran, T. V. (2003) Transition metal speciation in the cell: Insights from the chemistry of metal ion receptors. *Science 300*, 931–936.
36. Burns, C. S., Aronoff-Spencer, E., Legname, G., Prusiner, S. B., Antholine, W. E., Gerfen, G. J., Peisach, J., and Millhauser, G. L. (2003) Copper coordination in the full-length, recombinant prion protein. *Biochemistry 42*, 6794–6803.
37. Viles, J. H., Donne, D., Kroon, G., Prusiner, S. B., Cohen, F. E., Dyson, H. J., and Wright, P. E. (2001) Local structural plasticity of the prion protein. Analysis of NMR relaxation dynamics. *Biochemistry 40*, 2743–2753.
38. Jackson, G. S., Murray, I., Hosszu, L. L., Gibbs, N., Waltho, J. P., Clarke, A. R., and Collinge, J. (2001) Location and properties of metal-binding sites on the human prion protein. *Proc. Natl. Acad. Sci. U.S.A. 98*, 8531–8535.
39. Whittal, R. M., Ball, H. L., Cohen, F. E., Burlingame, A. L., Prusiner, S. B., and Baldwin, M. A. (2000) Copper binding to octarepeat peptides of the prion protein monitored by mass spectrometry. *Protein Sci. 9*, 332–343.
40. Sarell, C. J., Syme, C. D., Rigby, S. E., and Viles, J. H. (2009) Copper(II) binding to amyloid-β fibrils of Alzheimer's disease reveals a picomolar affinity: Stoichiometry and coordination geometry are independent of Aβ oligomeric form. *Biochemistry 48*, 4388–4402.
41. Yatsunyk, L. A., and Rosenzweig, A. C. (2007) Cu(I) Binding and Transfer by the N Terminus of the Wilson Disease Protein. *J. Biol. Chem. 282*, 8622–8631.
42. Wernimont, A. K., Yatsunyk, L. A., and Rosenzweig, A. C. (2004) Binding of copper(I) by the Wilson disease protein and its copper chaperone. *J. Biol. Chem. 279*, 12269–12276.
43. Miras, R., Morin, I., Jacquin, O., Cuillel, M., Guillain, F., and Mintz, E. (2008) Interplay between glutathione, Atx1 and copper. 1. Copper-(I) glutathionate induced dimerization of Atx1. *J. Biol. Inorg. Chem. 13*, 195–205.
44. Magyar, J. S., and Godwin, H. A. (2003) Spectropotentiometric analysis of metal binding to structural zinc-binding sites: Accounting quantitatively for pH and metal ion buffering effects. *Anal. Biochem. 320*, 39.
45. Yatsunyk, L., Easton, J., Kim, L., Sugarbaker, S., Bennett, B., Breece, R., Vorontsov, I., Tierney, D., Crowder, M., and Rosenzweig, A. (2008) Structure and metal binding properties of ZnuA, a periplasmic zinc transporter from *Escherichia coli*. *J. Biol. Inorg. Chem. 13*, 271–288.
46. Walkup, G. K., and Imperiali, B. (1997) Fluorescent Chemosensors for Divalent Zinc Based on Zinc Finger Domains. Enhanced Oxidative Stability, Metal Binding Affinity, and Structural and Functional Characterization. *J. Am. Chem. Soc. 119*, 3443–3450.
47. Hunt, J. B., Neece, S. H., and Ginsburg, A. (1985) The use of 4-(2-pyridylazo)resorcinol in studies of zinc release from *Escherichia coli* aspartate transcarbamoylase. *Anal. Biochem. 146*, 150–157.
48. Chong, L. X., Ash, M. R., Maher, M. J., Hinds, M. G., Xiao, Z., and Wedd, A. G. (2009) Unprecedented binding cooperativity between Cu(I) and Cu(II) in the copper resistance protein CopK from *Cupriavidus metallidurans* CH34: Implications from structural studies by NMR spectroscopy and X-ray crystallography. *J. Am. Chem. Soc. 131*, 3549–3564.
49. Zhou, L., Singleton, C., and LeÂ brun, N. E. (2008) High Cu(I) and low proton affinities of the CXXC motif of *Bacillus subtilis* CopZ. *Biochem. J. 413*, 459–465.
50. Djoko, K. Y., Xiao, Z., Huffman, D. L., and Wedd, A. G. (2007) Conserved Mechanism of Copper Binding and Transfer. A Comparison of the Copper-Resistance Proteins PcoC from *Escherichia coli* and CopC from *Pseudomonas syringae*. *Inorg. Chem. 46*, 4560–4568.
51. Zhang, L., Koay, M., Maher, M. J., Xiao, Z., and Wedd, A. G. (2006) Intermolecular Transfer of Copper Ions from the CopC Protein of *Pseudomonas syringae*. Crystal Structures of Fully Loaded Cu(I)Cu-(II) Forms. *J. Am. Chem. Soc. 128*, 5834–5850.
52. Borrelly, G. P. M., Rondet, S. A. M., Tottey, S., Robinson, N. J., and Axelsen, K. B. (2004) Chimeras of P1-type ATPases and their transcriptional regulators: Contributions of a cytosolic amino-terminal domain to metal specificity. *Mol. Microbiol. 53*, 217–227.
53. Himelblau, E., Mira, H., Lin, S.-J., Cizewski Culotta, V., Penarrubia, L., and Amasino, R. M. (1998) Identification of a Functional Homolog of the Yeast Copper Homeostasis Gene ATX1 from *Arabidopsis*. *Plant Physiol. 117*, 1227–1234.
54. Giedroc, D. P., and Arunkumar, A. I. (2007) Metal sensor proteins: Nature's metalloregulated allosteric switches. *Dalton Trans.,* 3107–3120.
55. Pollák, M., and Kubán, V. (1979) Comparison of Spectrophotometric Methods of Determination of Zinc(II) in Biological Material and Study of its Complex Formation Reactions with 4-(2-Pyridylazo)resorcinol. *Collect. Czech. Chem. Commun. 44*, 725–741.
56. Blair, D., and Diehl, H. (1961) Bathophenanthrolinedisulfonic Acid and Bathocuproinedisulfonic Acid, Water-Soluble Reagents for Iron and Copper. *Talanta 7*, 163–174.
57. Otwinowski, Z., and Minor, W. (1997) Processing of X-ray Diffraction Data Collected in Oscillation Mode. In Methods in Enzymology (Carter, C. W. J., and Sweet, R. M., Eds.) pp 307−326, Academic Press, San Diego.